ADVANCES IN ELECTRONICS AND ELECTRON PHYSICS, VOL. 88

Fractal Signal Analysis Using Mathematical Morphology

PETROS MARAGOS

School of Electrical Engineering, Georgia Institute of Technology, Atlanta, Georgia

I. Introduction

Natural scenes contain many classes of objects that have a high degree of geometrical complexity. Examples include clouds, mountains, trees, and coastlines. In addition, many nonlinear dynamical systems give rise to limit sets whose images exhibit a high degree of geometrical complexity. Mandelbrot (1982) has demonstrated in his pioneering work that a large

ISBN 0-12-014730-0

class of mathematical sets, called *fractals*, can model well many such image classes. Fractal images have become aesthetically attractive through synthesis via computer graphics (Mandelbrot, 1982; Voss, 1988; Barnsley, 1988). Although the fractal images are the most popularized class of fractals, there are also numerous natural processes described by time-series measurements (e.g., $1/f$ noises, econometric and demographic data, pitch variations in music signals) that are fractals (Mandelbrot, 1982; Voss, 1988). The one-dimensional (abbreviated as 1D)[1] signals representing these measurements are fractals in the sense that their graph is a fractal set. In addition, the geometrical complexity of fractal surfaces of physical objects is often inherited in the 2D image intensity signals emanating from such objects (Pentland, 1984). Thus, analyzing and modeling fractal signals is of great interest both from a scientific and an engineering viewpoint.

Perhaps the most important characteristic of fractals is that they have similar structure at multiple scales. Thus, in this chapter we address two problems related to this multiscale structure of fractal signals. The first is an analysis problem and deals with the estimation of the fractal dimension. This is an important parameter measuring the degree of fragmentation of fractal signals and is useful for their description and classification. Intuitively, it measures the degree of their fragmentation or irregularity over multiple scales. It makes meaningful the measurement of metric aspects such as the length of fractal curves and the area of surfaces. The second problem deals with modeling fractal images by collages, i.e., nonlinear combinations of down-scaled, rotated, and shifted versions of the original image. The unifying theme in the approaches presented herein to both problems is the extensive use of morphological filters for their efficiency as well as their ability to rigously extract size information from a signal at multiple scales. These morphological filters are based on elementary operators of morphological signal analysis (Serra, 1982; Maragos and Schafer, 1987, 1990).

This chapter begins by providing in Section II the definitions of some basic morphological transformations for sets and signals, i.e., the erosion, dilation, and opening operations, which are required for the analysis in this chapter. This is followed by a brief survey of the theory of fractal dimensions. There is a proliferation of fractal dimensions, all of which are more or less capable of measuring the degree of fragmentation of a signal's graph. In Section III we review their definitions and interrelationships. Emphasis is given on the Minkowski–Bouligand dimension, whose analysis is done using morphological operations. There are numerous classes of

[1] In this chapter the notation nD will mean "n-dimensional," where $n = 1, 2, 3, \ldots$. An nD signal will imply a function with n independent variables, whereas an nD set will mean a set of points in the Euclidean space $\mathbf{R}^n$.

fractal signals. In Section IV we review three classes of parametric fractal signals and related algorithms for their synthesis. The performance of the presented morphological method for measuring fractal dimension is tested by applying it to the above synthetic fractal signals.

Section V focuses on the covering methods, a class of general and efficient approaches to compute the fractal dimension of arbitrary fractal signals. It essentially reviews the work of Maragos and Sun (1991) where a general framework was presented, based on multiscale morphological erosions and dilations with varying structuring elements, that provides the theoretical support for and underlies many of the digital implementations of covering methods, e.g., in Dubuc *et al.* (1989) and the 1D analogs of the methods in Peleg *et al.* (1984), Stein (1987), and Peli *et al.* (1989). We shall refer to these unified algorithms as the *morphological covering method.* This approach originally attempts to cover the graph of a 1D signal with 2D sets at multiple scales. Thus, for an N-sample N-level 1D digital signal, the set-cover methods require a $O(N^2)$ computational complexity at each scale. However, covering the signal's graph with properly chosen 1D functions via morphological filtering yields identical results and involves 1D processing of the signal. Hence, the morphological filtering approach reduces the original set-cover complexity from quadratic to linear, since for an N-sample 1D signal the function-cover method has complexity $O(N)$ at each scale. A morphological covering algorithm for estimating the fractal dimension of discrete-time signals is also presented and applied to three classes of fractal signals. The morphological covering method applies to arbitrary signals. In Section V.D we briefly describe (from Maragos , 1991) its application to measuring the short-time fractal dimension of speech signals. Section VI extends the morphological covering approach to finding the fractal dimension of 2D signals and provides a related discrete algorithm. Section VII deals with modeling fractal binary images using collages. The theory of collages is first reviewed from Barnsley (1988) and then an approach is presented from Libeskind-Hadas and Maragos (1987) to finding a good collage based on morphological skeletonization. Finally, Section VIII concludes with some suggestions for future work.

II. Morphological Signal Transformations

In this section we review the definitions of the elementary morphological transformations for sets and signals. More details, the properties, and many applications of these operators can be found in Serra (1982), Sternberg (1986), Maragos and Schafer (1987, 1990), Haralick *et al.* (1987), Heijmans and Ronse (1988), and Serra and Vincent (1992).

A. Set Operations

Consider sets X, B in the Euclidean space $\mathbf{R}^d$ or the discrete space $\mathbf{Z}^d$, $d = 1, 2, 3, \ldots$, where $\mathbf{R}$ is the set of reals and $\mathbf{Z}$ is the set of all integers. Let

$$X \pm z \triangleq \{x \pm z : x \in X\} \tag{1}$$

denote the translate of X by the vector $\pm z$, and let $\check{B} \triangleq \{-b : b \in B\}$ be the reflection of B. The fundamental morphological operators for sets are the dilation $\oplus$ and erosion $\ominus$ of X by B, which are defined as follows:

$$X \oplus B \triangleq \bigcup_{b \in B} X + b = \{z : (\check{B} + z) \cap X \neq \emptyset\} \tag{2}$$

$$X \ominus B \triangleq \bigcap_{b \in B} X - b = \{z : B + z \subseteq X\} \tag{3}$$

In applications where X is an input set to some system, the second set B is usually compact and has a simple shape and small size; B is then called a *structuring element*. Thus, the output of the dilation operator is the set of translation points such that the translate of the reflection of B has a nonempty intersection with the input set. Similarly, the output of the erosion operator is the set of translation points such that the translated structuring element is contained in the input set.

Another fundamental operator is the opening $\bigcirc$ of X by B:

$$X \bigcirc B \triangleq (X \ominus B) \oplus B \tag{4}$$

Note that $X \bigcirc B \subseteq X$ for all X and B, because

$$X \bigcirc B = \bigcup_{b+z \subseteq X} B + z \tag{5}$$

To visualize the geometrical behavior of these operators, it is helpful to consider a 2D set X representing a binary image and the structuring element B being a disk centered at the origin. Then the erosion shrinks the set X, whereas dilation expands X. The opening suppresses the sharp capes and cuts the narrow isthmuses of X, inside which B cannot fit. Thus the opening by a disk performs a nonlinear smoothing of the image contour. Clearly, if we vary the structuring element B, then its shape and size will determine the nature and the degree of shrinking, expansion, or smoothing during the above morphological operations.

B. Function Operations

Consider signals f and g whose domain is the set $\mathbf{E}$, equal either to the Euclidean space $\mathbf{R}^d$, $d = 1, 2, 3, \ldots$, or the discrete space $\mathbf{Z}^d$, and whose range is a subset of $\mathbf{R} \cup \{-\infty, \infty\}$. The support of f is the following subset of its domain:

$$\mathrm{Spt}(f) \triangleq \{x \in \mathbf{E} : f(x) > -\infty\} \tag{6}$$

The dilation $\oplus$ and $\ominus$ of the signal f by the (structuring) signal g are defined as the signal operations

$$(f \oplus g)(x) \triangleq \sup_{y \in \check{G}+x} \{f(y) + g(x - y)\} \tag{7}$$

$$(f \ominus g)(x) \triangleq \inf_{y \in G+x} \{f(y) - g(y - x)\} \tag{8}$$

where

$$G = \mathrm{Spt}(g) \tag{9}$$

The structuring function g usually has a compact support G and simple shape.

A special, but quite useful in applications, case results when g is a flat function, i.e., assumes only two values on $\mathbf{E}$. Specficially if

$$g(x) = \begin{cases} 0, & \text{if } x \in G \\ -\infty, & \text{if } x \notin G \end{cases} \tag{10}$$

then the general dilation and erosion of f by g reduce to the following moving local maxima and minima:

$$(f \oplus g)(x) = \sup_{y \in G} \{f(x - y)\} \tag{11}$$

$$(f \ominus g)(x) = \inf_{y \in G} \{f(x + y)\} \tag{12}$$

III. Fractal Dimensions

In this section we review several fractal dimensions,[2] which are more or less capable of quantifying the degree of fragmentation of curves and surfaces. More general and detailed discussions on these topics can be found in the books by Mandelbrot (1982), Barnsley (1988), and Falconer (1990).

Unless otherwise stated, we shall assume in this section that F is a nonempty compact subset of the Euclidean space $\mathbf{R}^d$, $d = 1, 2, 3, \ldots$

[2] All the fractal dimensions discussed in this chapter are related only to the geometry of a set and its metric aspects. For fractals that are sets of attracting points of chaotic dynamical systems, Farmer *et al.* (1983) discuss other types of dimensions that depend on the probability mass of parts of the set; such dimensions are not discussed in this chapter.

A. Hausdorff Dimension

Let $\varepsilon \geq 0$ be the scale parameter. An ε-cover of F is any countable set collection $\mathcal{K}(\varepsilon) = \{X_i : i = 1, 2, \ldots\}$ such that $F \subseteq \bigcup_i X_i$ and $0 < \text{diam}(X_i) \leq \varepsilon$ for all i, where $\text{diam}(X_i)$ is the largest distance between any two points of X_i. The δ-dimensional Hausdorff measure of F is defined as

$$\mathcal{H}_\delta(F) = \lim_{\varepsilon \to 0} \left(c_\delta \inf_{\mathcal{K}(\varepsilon)} \left\{ \sum_i [\text{diam}(X_i)]^\delta \right\} \right) \tag{13}$$

where $c_\delta = \gamma(\delta)/2^\delta$ is a normalizing constant and

$$\gamma(\delta) = \frac{[\Gamma(1/2)]^\delta}{\Gamma(1 + 0.5\delta)} \tag{14}$$

where $\Gamma(\,)$ is the gamma function.[3] Note that, if $d = 1, 2, 3, \ldots$, then $\gamma(d)\varepsilon^d$ is the volume of the d-dimensional ball of radius ε. There is a critical real number $D_H \geq 0$ such that

$$\mathcal{H}_\delta = \begin{cases} \infty, & \delta < D_H \\ 0, & \delta > D_H \end{cases} \tag{15}$$

This critical D_H is the Hausdorff dimension of F and is equal to

$$D_H(F) = \inf\{\delta : \mathcal{H}_\delta(F) = 0\} \tag{16}$$

This dimension was introduced by Hausdorff (1918) and further analyzed by Besicovitch (1934) and Besicovitch and Ursell (1937). Mandelbrot (1982) defines formally the fractal dimension of F as equal to D_H. Further, he calls a set fractal if D_H strictly exceeds its topological dimension D_T. Hence

$$\text{set } F \text{ is fractal} \Leftrightarrow \text{Hausdorff dim } D_H(F) > \text{topological dim } D_T(F)$$

The topological dimension is always an integer, and for a continuous curve represented by a function, D_T is the number of independent variables of this function. Whenever the set F is implied, we will drop it as argument of the various dimensions. General categories of fractal sets in $\mathbf{R}^3$ are:

$$D_T = 0 < D_H \leq 1 \Rightarrow F = \text{fractal dust}$$

$$D_T = 1 < D_H \leq 2 \Rightarrow F = \text{fractal curve}$$

$$D_T = 2 < D_H \leq 3 \Rightarrow F = \text{fractal surface}$$

[3] The gamma function is defined as $\Gamma(p) = \int_0^\infty x^{p-1} \exp(-x)\, dx$, $0 < p < \infty$. Note that $\Gamma(1/2) = \sqrt{\pi}$, and $\Gamma(a + n) = (a + n - 1)(a + n - 2) \ldots a\Gamma(a)$ for $n = 1, 2, 3, \ldots$ and $0 < a \leq 1$.

Example 1. Cantor set: Define a set sequence $\{C_n\}_{n=0}^\infty$ through the following recursion:

$$C_0 = [0, 1] = \{r \in \mathbf{R} : 0 \leq r \leq 1\} \tag{17}$$

$$C_1 = [0, \tfrac{1}{3}] \cup [\tfrac{2}{3}, 1] \tag{18}$$

$$C_2 = [0, \tfrac{1}{9}] \cup [\tfrac{2}{9}, \tfrac{3}{9}] \cup [\tfrac{6}{9}, \tfrac{7}{9}] \cup [\tfrac{8}{9}, 1] \tag{19}$$

$$\vdots \quad \vdots \quad \vdots$$

$$C_n = (\tfrac{1}{3}C_{n-1}) \cup [(\tfrac{1}{3}C_{n-1}) + \tfrac{2}{3}], \qquad n = 1, 2, 3, \ldots \tag{20}$$

where, given an arbitrary set $X \subseteq \mathbf{R}^d$, $d = 1, 2, 3, \ldots$, the set

$$rX \triangleq \{rx : x \in X\} \tag{21}$$

is its scaling (i.e., positive homothetic) by the real number $r > 0$. Thus, each member of the sequence C_n is equal to the union of two scalings of C_{n-1} by 1/3, one of which is also translated by the vector 2/3. The sequence $\{C_n\}$ is a monotonically decreasing sequence of closed sets whose limit

$$C = \lim_{n \to \infty} C_n = \bigcap_n C_n \tag{22}$$

is the *Cantor set*. At each n, C_n consists of 2^n intervals of length

$$\varepsilon_n = (\tfrac{1}{3})^n \tag{23}$$

The Hausdorff measure can be found as

$$\mathcal{H}_\delta = \lim_{n \to \infty} c_\delta H(\varepsilon_n, \delta) \tag{24}$$

where

$$H(\varepsilon_n, \delta) \triangleq \inf_{\mathcal{K}(\varepsilon_n)} \left\{ \sum_i [\text{diam}(X_i)]^\delta \right\} \tag{25}$$

In general, the tightest covers $\mathcal{K}(\varepsilon_n)$ will be when, for each i, $\text{diam}(X_i) = (1/3)^{n_i}$ for some integer $n_i \geq n$. If $2 > 3^\delta$, then the tightest cover occurs if $n_i = n$ for all i, because using $\text{diam}(X_i) = (1/3)^{n'}$ with $n' > n$ for some i yields

$$\left(\frac{2}{3^\delta}\right)^{n'} \geq \sum_i [\text{diam}(X_i)]^\delta \geq \left(\frac{2}{3^\delta}\right)^n$$

Therefore,

$$H(\varepsilon_n, \delta) = (2/3^\delta)^n$$

and hence

$$\mathcal{H}_\delta = \lim_{n \to \infty} \left(\frac{2}{3^\delta}\right)^n = \infty$$

Further, we have

$$\frac{2}{3^\delta} < 1 \Rightarrow H(\varepsilon_n, \delta) \le \left(\frac{2}{3^\delta}\right)^n \Rightarrow \mathcal{H}_\delta = 0$$

Since

$$\mathcal{H}_\delta = \begin{cases} 0, & \text{if } \delta > \log(2)/\log(3) \\ \infty, & \text{if } \delta < \log(2)/\log(3) \end{cases}$$

the Hausdorff dimension of the Cantor set is

$$D_H(C) = \frac{\log(2)}{\log(3)} = 0.6309$$

B. Similarity Dimension

If F can be decomposed into the union of n disjoint of just-touching copies of itself that are (possibly translated, rotated, and) scaled by ratios r_i, $i = 1, \ldots, n$, then the similarity dimension (Mandelbrot, 1982) is the solution D_S of the equation

$$\sum_{i=1}^{n} r_i^{D_S} = 1 \tag{26}$$

If all ratios r_i are equal to $r = r_i$, then

$$D_S = \frac{\log(N)}{\log(1/r)} \tag{27}$$

In several cases we have $D_S = D_H$ (Hutchinson, 1981; Mandelbrot, 1982).

Example 2. Consider the Cantor set C defined as the limit of the set sequence C_n in (20). Since each C_n is the union of $N = 2$ copies of C_{n-1} scaled by $r = 1/3$, the limit C will be the union of two copies of itself scaled by 1/3. Hence

$$D_S(C) = \frac{\log(2)}{\log(3)}$$

C. Minkowski–Bouligand Dimension

1. *Sets in* $\mathbf{R}^3$

This dimension is based conceptually on an idea by Minkowski (1901, 1903) of finding the area of irregular surfaces or length of irregular curves F in $\mathbf{R}^3$. Specifically, dilate F with spheres of radius ε by forming the union of these spheres centered at all points of F and thus create the set

$$F_\varepsilon = \bigcup_{z \in F} \{(\varepsilon b + z) \in \mathbf{R}^3 : \|b\| \le 1\}, \qquad \varepsilon \ge 0 \tag{28}$$

where, for $d = 1, 2, 3, \ldots$, $\|\cdot\|$ is the Euclidean norm

$$\|b\| \triangleq \sqrt{b_1^2 + \cdots + b_d^2}, \qquad b = (b_1, \ldots, b_d) \in \mathbf{R}^d \tag{29}$$

F_ε is called a *Minkowski cover.*[4] Then find the volume $\text{vol}(F_\varepsilon)$ of the dilated set at all scales ε, and set the volume, area, and length of the original set F as equal to[5]

$$\begin{aligned} \text{vol}(F) &= \lim_{\varepsilon \to 0} \text{vol}(F_\varepsilon) \\ \text{area}(F) &= \lim_{\varepsilon \to 0} \text{vol}(F_\varepsilon)/2\varepsilon \\ \text{len}(F) &= \lim_{\varepsilon \to 0} \text{vol}(F_\varepsilon)/\pi\varepsilon^2 \end{aligned} \tag{30}$$

For $d = 1, 2, 3, \ldots$, it follows from (14) that the volume of a d-dimensional ball of radius ε is

$$\gamma(d)\varepsilon^d = \{(\varepsilon b) \in \mathbf{R}^d : \|b\| \le 1\} \tag{31}$$

Now the Minkowski δ-content of F is defined as

$$\delta\text{-content of } F \triangleq \lim_{\varepsilon \to 0} \frac{\text{vol}(F_\varepsilon)}{\gamma(3 - \delta)\varepsilon^{3-\delta}} \tag{32}$$

Example 3. Square: If S is the square

$$S = \boxed{\ l\ }$$

then

$$\text{vol}(S_\varepsilon) = 2l^2\varepsilon + 2\pi l\varepsilon^2 + 4\pi\varepsilon^3/3$$

and

δ	1	2	3
δ-content	length $= \infty$	area $= l^2$	volume $= 0$

Thus, in general, for any set F there is a critical number D_M such that

$$\delta\text{-content of } F = \begin{cases} \infty, & \text{if } \delta < D_M \\ 0, & \text{if } \delta > D_M \end{cases} \tag{33}$$

[4] Bouligand (1928) and Mandelbrot (1982) attribute this cover construction also to Cantor.

[5] Serra (1982) also has a related discussion where morphological dilations are used in stereology.

Bouligand (1928) extended these ideas to cases where D_M is not only integer but also fractional. Hence, the *Minkowski–Bouligand dimension* is defined as

$$D_M(F) \triangleq \inf\left\{\delta : \lim_{\varepsilon \to 0} \frac{\text{vol}(F_\varepsilon)}{\gamma(3-\delta)\varepsilon^{3-\delta}} = 0\right\} \tag{34}$$

$$= 3 - \lambda[\text{vol}(F_\varepsilon)] \tag{35}$$

where we define

$$\lambda(f) \triangleq \sup\left\{p : \lim_{x \to 0} \frac{f(x)}{x^p} = 0\right\} \tag{36}$$

as the infinitesimal order of a function $f(x)$, around $x = 0$.

Lemma 4. *The infinitesimal order of a function $f(x)$ can be obtained by*

$$\lambda(f) = \lim_{|x| \to 0} \frac{\log(|f(x)|)}{\log(|x|)} \tag{37}$$

Proof. If we denote

$$P = \left\{p : \lim_{x \to 0} f(x)x^{-p} = 0\right\}$$

then

$$\lambda = \sup\{p : p \in P\}$$

Note that $p \in P$ if and only if for all $\varepsilon > 0$ there exists a $\delta > 0$ such that $|f(x)| \le \varepsilon |x|^p$ and hence

$$\log(|f(x)|) \le p \log(|x|) + \log(\varepsilon), \qquad |x| < \delta$$

This implies

$$p \le \frac{\log(|f(x)|)}{\log(|x|)} - \frac{\log(\varepsilon)}{\log(|x|)}, \qquad |x| < \min(1, \delta)$$

Thus in the limit $|x| \to 0$ we obtain

$$p \le \lim_{|x| \to 0} \frac{\log(|f(x)|)}{\log(|x|)}$$

Since also $p \in P$ implies that $p - \varepsilon \in P$ for all $\varepsilon > 0$, the above analysis implies that

$$\lambda = \sup\left\{p : p \le \lim_{|x| \to 0} \frac{\log(|f(x)|)}{\log(|x|)}\right\}$$

which completes the proof of (37). (*Q.E.D.*)

From the above lemma it follows that

$$\lambda[\text{vol}(F_\varepsilon)] = \lim_{\varepsilon \to 0} \frac{\log[\text{vol}(F_\varepsilon)]}{\log(\varepsilon)} \tag{38}$$

which implies that

$$D_M(F) = \lim_{\varepsilon \to 0} \frac{\log[\text{vol}(F_\varepsilon)/\varepsilon^3]}{\log(1/\varepsilon)} \tag{39}$$

It is also possible to replace the limit $\varepsilon \to 0$ with the limit of a sequence; i.e.,

$$D_M(F) = \lim_{n \to \infty} \frac{\log[\text{vol}(F_{\varepsilon_n})/\varepsilon_n^3]}{\log(1/\varepsilon_n)} \tag{40}$$

where $\{\varepsilon_n\}_{n=0}^{\infty}$ is a decreasing sequence of scales such that $\varepsilon_n = pr^n$ for all n, for some $0 < r < 1$ and $p > 0$.

The intuitive meaning of the dimension $D = D_M$ is that

$$\begin{aligned} \text{vol}(F_\varepsilon) &\approx c_1 \varepsilon^\lambda, \\ \text{area}(F_\varepsilon) &\approx c_2 \varepsilon^{2-D}, \qquad \text{as } \varepsilon \to 0 \\ \text{len}(F_\varepsilon) &\approx c_3 \varepsilon^{1-D}, \end{aligned} \tag{41}$$

where c_1, c_2, c_3 are proportionality constants. Thus if F is a curve in $\mathbf{R}^3$ and $D > 1$, then its length is infinite.

2. *Sets in* $\mathbf{R}^2$

To find the area and length of a compact set $F \subseteq \mathbf{R}^2$ we can create a 2D Minkowski cover

$$F_\varepsilon = \bigcup_{z \in F} \{(\varepsilon b + z) \in \mathbf{R}^2 : \|b\| \le 1\} \tag{42}$$

by dilating F with disks of radius ε, find the area of the dilated set at all scales ε, and set the area and length of the original set F as equal to

$$\begin{aligned} \text{area}(F) &= \lim_{\varepsilon \to 0} \text{area}(F_\varepsilon) \\ \text{len}(F) &= \lim_{\varepsilon \to 0} \text{area}(F_\varepsilon)/2\varepsilon \end{aligned} \tag{43}$$

Then the Minkowski–Bouligand dimension of F is equal to

$$D_M(F) \triangleq 2 - \lambda[\text{area}(F_\varepsilon)] \tag{44}$$

$$= \lim_{\varepsilon \to 0} \frac{\log[\text{area}(F_\varepsilon)/\varepsilon^2]}{\log(1/\varepsilon)} \tag{45}$$

Example 5. Linear Segment: Consider the 1D set

$$S = \underline{\quad l \quad}$$

Then the Minkowski cover area is

$$\text{area}(S_\varepsilon) = 2l\varepsilon + \pi\varepsilon^2$$

Hence

$$D_M(S) = 2 - \lambda[\text{area}(S_\varepsilon)] = 2 - 1 = 1$$

3. *Sets in* $\mathbf{R}$

To find the length of a compact set $F \subseteq \mathbf{R}$ we can create a 1D Minkowski cover

$$F_\varepsilon = \bigcup_{z \in F} \{(\varepsilon b + z) \in \mathbf{R} : -1 \le b \le 1\} \tag{46}$$

by dilating F with intervals $[-\varepsilon, \varepsilon]$, and set the length of the original set F as equal to

$$\text{len}(F) = \lim_{\varepsilon \to 0} \text{len}(F_\varepsilon) \tag{47}$$

Then the Minkowski–Bouligand dimension of F is equal to

$$D_M(F) \triangleq 1 - \lambda[\text{len}(F_\varepsilon)]$$

$$= \lim_{\varepsilon \to 0} \frac{\log[\text{len}(F_\varepsilon)/\varepsilon]}{\log(1/\varepsilon)} \tag{49}$$

Example 6. Consider the Cantor set C, which is the limit of the set sequence $\{C_n\}$ defined in (20). Since $C_{n+1} \subseteq C_n$ for all n and $C = \bigcap_n C_n$,

$$C_\varepsilon = \bigcap_n (C_n)_\varepsilon \tag{50}$$

Dilating each C_k with an interval $[-\varepsilon_n, \varepsilon_n]$, where $2\varepsilon_n = (1/3)^n$, creates the dilated sets

$$(C_k)_{\varepsilon_n} = (C_{n-1})_{\varepsilon_n} \qquad \forall\, k \ge n - 1 \tag{51}$$

Hence the 1D Minkowski cover of C at scale ε_n has length

$$\text{len}(C_{\varepsilon_n}) = 2^{n-1}\left(\frac{1}{3^{n-1}} + 2\varepsilon_n\right) = 2\left(\frac{2}{3}\right)^n \tag{52}$$

which implies that

$$D_M(C) = \lim_{n \to \infty} \frac{\log[\text{len}(C_{\varepsilon_n})/\varepsilon_n]}{\log(1/\varepsilon_n)} = \lim_{n \to \infty} \frac{\log(4 \cdot 2^n)}{\log(2 \cdot 3^n)} = \frac{\log(2)}{\log(3)} \tag{53}$$

D. Box-Counting Dimension

For compact planar set $F \subseteq \mathbf{R}^2$ let us partition the plane with a grid of square boxes of side ε and count the number $N(\varepsilon)$ of boxes that intersect that set F. Then, if we replace the Minkowski cover area in (45) with the box cover area

$$A_{boxc}(F, \varepsilon) \triangleq \varepsilon^2 N(\varepsilon) \tag{54}$$

we obtain the *box dimension* (Bouligand, 1928)

$$D_B(F) \triangleq 2 - \lambda[A_{boxc}(F, \varepsilon)] = \lim_{\varepsilon \to 0} \frac{\log[A_{boxc}(F, \varepsilon)/\varepsilon^2]}{\log(1/\varepsilon)} \tag{55}$$

$$= \lim_{\varepsilon \to 0} \frac{\log[N(\varepsilon)]}{\log(1/\varepsilon)} \tag{56}$$

Lemma 7. *For any compact set $F \subseteq \mathbf{R}^2$, the Minkowski cover area and the box cover area have the same infinitesimal order.*

Proof. Every disk of radius 2ε in the Minkowski cover of F will contain as subset the grid box that contains the coresponding disk center. Hence

$$A_{boxc}(F, \varepsilon) \le \text{area}(F_{2\varepsilon}) \tag{57}$$

Also, Bouligand (1928) has shown that $\text{area}(F_{r\varepsilon}) \ge r^2\ \text{area}(F_\varepsilon)$ for $0 \le r \le 1$, which implies that

$$\text{area}(F_\varepsilon) \ge \tfrac{1}{4}\,\text{area}(F_{2\varepsilon}) \tag{58}$$

In addition, every disk of radius ε in the Minkowski cover of F is a subset of the union of the box that contains the disk center and its eight neighbors; hence

$$\text{area}(F_\varepsilon) \le 9A_{boxc}(F, \varepsilon) \tag{59}$$

The three above inequalities imply that

$$\frac{\text{area}(F_\varepsilon)}{9} \le A_{boxc}(F, \varepsilon) \le 4 \cdot \text{area}(F_\varepsilon) \tag{60}$$

Taking logarithms on all sides of this inequality, dividing by $\log(\varepsilon)$, and taking the limit as $\varepsilon \to 0$ yields

$$\lim_{\varepsilon \to 0} \frac{\log[\text{area}(F_\varepsilon)]}{\log(\varepsilon)} = \lim_{\varepsilon \to 0} \frac{\log[A_{boxc}(F, \varepsilon)]}{\log(\varepsilon)} \tag{61}$$

which implies that

$$\lambda[A_{boxc}(F, \varepsilon)] = \lambda[\text{area}(F_\varepsilon)] \tag{62}$$

This completes the proof of the lemma. (*Q.E.D.*)

As a direct corollary of the above lemma, we see that $D_B = D_M$ for all planar sets F. The definitions and results in this section can also be extended to compact sets $F \subseteq \mathbf{R}^d$ of any dimensionality $d = 1, 2, 3, \ldots$. For $d = 1$ the boxes will become intervals of length ε, whereas for $d = 3$, the boxes will become cubes of side ε. Thus, in general,

$$D_B = D_M \tag{63}$$

E. Entropy Dimension

The *entropy dimension* (Kolmogorov and Tihomirov, 1959) of a compact set $F \subseteq \mathbf{R}^d$ is defined as

$$D_E = \lim_{\varepsilon \to 0} \frac{\log[N_{min}(\varepsilon)]}{\log(1/\varepsilon)} \tag{64}$$

where $N_{min}(\varepsilon)$ is the smallest number of d-dimensional balls with radii ε required to cover F. (It is also called the "capacity" dimension in Farmer *et al.* (1983).) In Barnsley (1988) and in Falconer (1990) it is shown that

$$D_E = D_B \tag{65}$$

Example 8. Consider the Cantor set C, which is the limit of the set sequence $\{C_n\}$ defined in (20). Each set C_n consists of 2^n intervals of length $2\varepsilon_n = (1/3)^n$. For each scale ε_n, the smallest cover of C will be the set C_n, which consists of $N_{min}(\varepsilon) = 2^n$ intervals of length $2\varepsilon_n$. Hence

$$D_E(C) = \lim_{n \to \infty} \frac{\log[N_{min}(\varepsilon_n)]}{\log(1/\varepsilon_n)} = \lim_{n \to \infty} \frac{\log(2^n)}{\log(2 \cdot 3^n)} = \frac{\log(2)}{\log(3)} \tag{66}$$

F. Relations among Dimensions

For each compact subset of $\mathbf{R}^d$, the dimensions discussed in the previous sections satisfy the general relationships

$$0 \le D_T \le D_H \le D_M = D_B = D_E \le d$$
$$D_H \le D_S \tag{67}$$

In general, $D_H \neq D_M$ (Mandelbrot, 1985; McMullen, 1984; Falconer, 1990). However, in this chapter we focus on the Minkowski–Bouligand dimension D_M, which we shall henceforth call fractal dimension D, because; (1) it is clearly related to D_H, and hence able to quantify the fractal aspects of a signal, (2) it concides (in the continuous case) with D_H in many cases of practical interest; (3) it is much easier to compute than D_H; (4) it is more robust to compute than D_B for discrete-variable signals.

Although $D_B = D_M$ in the continuous case, they correspond to two different algorithms (with different performances) in the discrete case. In general, D_M can be more robustly estimated than D_B, which suffers from uncertainties due to the grid translation or its spacing. This is further explained in Section V.C.

In conclusion, a practical algorithm to estimate the dimension D_M is from the slope of the following approximately linear relation in $\log(1/\varepsilon)$; i.e., for sets $F \subseteq \mathbf{R}^3$:

$$\log\left[\frac{\text{vol}(F_\varepsilon)}{\varepsilon^3}\right] \approx D_M \cdot \log\left(\frac{1}{\varepsilon}\right) + \text{constant}, \qquad \text{as } \varepsilon \to 0 \tag{68}$$

and for planar sets $F \subseteq \mathbf{R}^2$:

$$\log\left[\frac{\text{area}(F_\varepsilon)}{\varepsilon^2}\right] \approx D_M \cdot \log\left(\frac{1}{\varepsilon}\right) + \text{constant}, \qquad \text{as } \varepsilon \to 0 \tag{69}$$

IV. Fractal Signals

A d-dimensional signal represented by a function $f: \mathbf{R}^d \to \mathbf{R}$ is called fractal if its graph

$$\text{Gr}(f) \triangleq \{(x, y) \in \mathbf{R}^d \times \mathbf{R} : y = f(x)\} \tag{70}$$

is a fractal set in $\mathbf{R}^{d+1}$. Further, if f is continuous, then its graph is a continuous curve with topological dimension equal to d. Hence

$$f \text{ is continuous} \Rightarrow d \le D_H[\text{Gr}(f)] \le D_M[\text{Gr}(f)] \le d + 1 \tag{71}$$

In this section we briefly describe three classes of parametric fractal test signals. These are the deterministic Weierstrass functions (WCFs) (Hardy, 1916; Mandelbrot, 1982; Berry and Lewis, 1980), the deterministic fractal interpolation functions (FIFs) (Barnsley, 1986: Barnsley, 1988; Hutchinson, 1981), and the random functions of fractional Brownian motion (FBM) (Mandelbrot and van Ness, 1968; Mandelbrot, 1982). These factals have been used in a variety of applications. For example, there are many natural phenomena that can be modeled using such parametric fractals (Mandelbrot, 1982). In addition, the FBM and FIFs have proven to be valuable in computer synthesis of images of natural scenes (Voss, 1988; Barnsley, 1988).

A. Weierstrass Function

The *Weierstrass cosine function* (WCF) is defined as

$$W_H(t) = \sum_{k=0}^{\infty} \gamma^{-kH} \cos(2\pi\gamma^k t) \tag{72}$$

with real positive parameters H and γ which, for convergence of the above infinite series, should be in the ranges

$$0 < H < 1, \qquad \gamma > 1$$

If γ is integer, then the WCF is periodic with period one. This function is continuous, but nowhere differentiable because its derivative is given by the infinite series

$$\frac{dW_H(t)}{dt} = -2\pi \sum_{k=0}^{\infty} \beta^k \sin(2\pi\gamma^k t), \qquad \beta = \gamma^{1-H} \tag{73}$$

which generally diverges since $\beta > 1$. The fractal dimension of the WCF is $D = 2 - H$.

In our computer experiments, we synthesized discrete-time signals from WCFs by sampling $t \in [0, 1]$ at $N + 1$ equidistant points, using a fixed $\gamma = 5$, and truncating the infinite series so that the summation is done only for $0 \le k \le k_{max}$, where k_{max} was determined by requiring $2\pi\gamma^k \le 10^{12}$, so that the cosine's argument does not exceed the computer's double-precision. Figure 1*a* shows three sampled WCFs whose fragmentation increases with their dimension D.

B. Fractal Interpolation Functions

The basic ideas in the theory of fractal interpolation functions were developed by Hutchinson (1981) and Barnsley (1986). Given is a set of data points $\{(x_k, y_k) \in \mathbf{R}^2; k = 0, 1, 2, \ldots, K > 1\}$ on the plane, where $x_{k-1} < x_k$ for all k. In the complete metric space $\mathcal{Q}$ of all continuous functions $q: [x_0, x_K] \to \mathbf{R}$ such that $q(x_0) = y_0$ and $q(x_K) = y_K$ define the function mapping Ψ by

$$\Psi(q)(x) = c_k\left(\frac{x - b_k}{a_k}\right) + V_k q\left(\frac{x - b_k}{a_k}\right) + d_k, \qquad x \in [x_{k-1}, x_k] \tag{74}$$

where $k = 1, 2, \ldots, K$, the $V_k \in (-1, 1)$ are free parameters, and the $4K$ parameters a_k, b_k, c_k, d_k are uniquely determined by

$$a_k x_0 + b_k = x_{k-1}, \qquad a_k x_K + b_k = x_k \tag{75}$$

$$V_k y_0 + c_k x_0 + d_k = y_{k-1}, \qquad V_k y_K + c_k x_K + d_k = y_k \tag{76}$$

Under the action of Ψ the graph of the input function q is mapped to the graph of the output $\Psi(q)$ via affine mappings

$$(x, y) \mapsto (ax + b, Vy + cx + d),$$

which include contractions and shifts of the domain and range of q. Ψ is a contraction mapping in $\mathcal{Q}$ and has a unique fixed point that is a

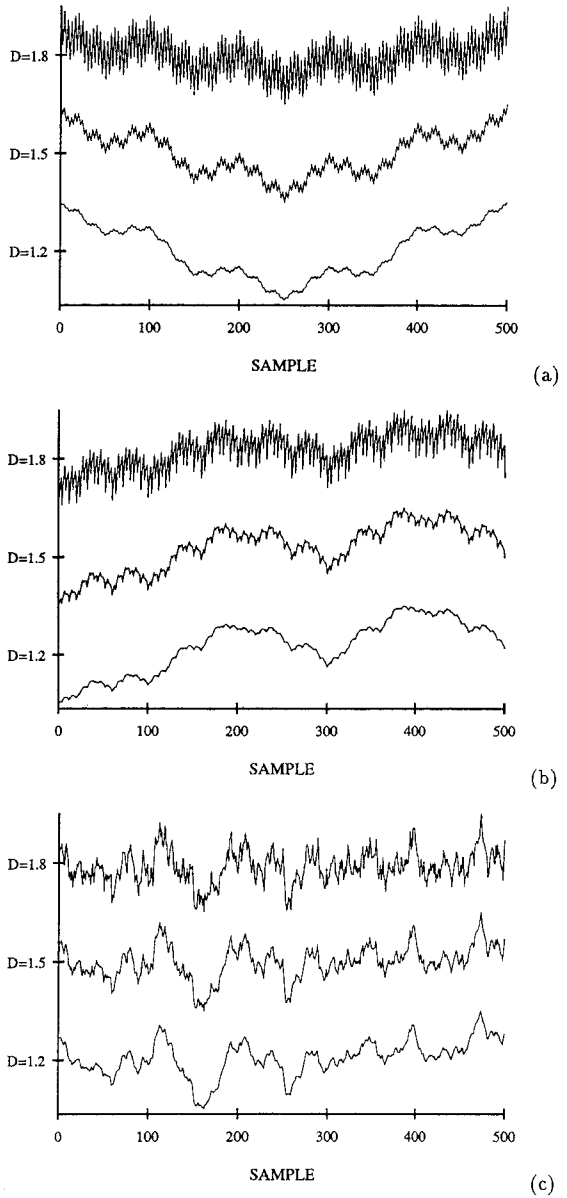

FIGURE 1. (a) Signals from sampling WCFs over [0, 1] with $\gamma = 5$ and various D. (b) Signals from sampling FIFs that interpolate the sequence 0, 1, 4, 2, 5, 3 with various D. (c) FBM signals obtained via a 512-point inverse FFT on random spectra with average magnitude $\propto |\omega|^{D-2.5}$. All three signals in each class have $N = 500$ and are scaled to have the same amplitude range. (From Maragos and Sun, 1991);

continuous function $F: [x_0, x_K] \to \mathbf{R}$ that interpolates the given data; i.e., $F(x_k) = y_k$ for $k = 0, 1, \ldots, K$. F is called a *fractal interpolation function* (FIF)[6] because quite often the fractal dimension D of its graph exceeds 1. Specifically (Barnsley, 1988; Hardin and Massopust, 1986), if $\sum_{k=1}^{K} |V_k| > 1$ and (x_k, y_k) are not all collinear, then D is the unique real solution of

$$\sum_{k=1}^{K} |V_k| a_k^{D-1} = 1 \tag{77}$$

Otherwise, $D = 1$. Thus by choosing the vertical scaling ratios V_k's we can synthesize a fractal interpolation function of any desired fractal dimension. F can be synthesized by iterating Ψ on any initial function q in $\mathcal{Q}$; i.e., $F = \lim_{n\to\infty} \Psi^{on}(q)$ where $\Psi^{on}(q) = \Psi[\Psi^{o(n-1)}(q)]$.

Given a finite-length discrete-time signal $f_o[k]$, $k = 0, 1, \ldots, K$, an algorithm was described in Maragos (1991) to fractally interpolate f_o by an integer factor M by sampling a FIF whose fractal dimension can be controlled via a single parameter. Specifically, we start from the $K + 1$ data pairs $(x_k = kM, y_k = f_o[k])$ with $x_K = MK = N$, set $a_k = 1/K$, $b_k = x_{k-1}$, and select a constant $V_k = V \in (-1, 1)$, where

$$|V| = K^{D-2}, \qquad 1 < D < 2 \tag{78}$$

Then there is a unique fractal interpolation function $F_D: [0, N] \to \mathbf{R}$ with fractal dimension D, which interpolates the given data, i.e., $F_D(kM) = f_o[k]$. In our computer experiments we synthesize F_D by iterating Ψ starting from some initial $q \in \mathcal{Q}$ until the maximum absolute error between successive iterations becomes very small, i.e., smaller than 10^{-10}. If $V = 0$, F_D is the piece-linear interpolant of the data. The graph of F_D has fractal dimension

$$D = \begin{cases} 2 + \log(|V|)/\log(K) & \text{if } 1 > |V| > 1/K \\ 1 & \text{if } |V| \le 1/K \end{cases} \tag{79}$$

Based on F_D we can up-sample f_o to a $1:M$ interpolated signal $F_D(n)$, $n = 0, 1, \ldots, N$. The larger $|V|$ is, the larger D, and the more fragmented F_D. Figure 1*b* shows examples of FIFs that interpolate a fixed data sequence of $K + 1 = 6$ points by a factor $M = 100$ using positive ratios $V = 5^{D-2}$.

C. Fractional Brownian Motion

The *fractional Brownian motion* (FBM) (Mandelbrot and van Ness, 1968) $B_H(t)$ with parameter $0 < H < 1$ is a time-varying random function with stationary, Gaussian-distributed, and statistically self-affine increments; the latter means that $[B_H(t + T) - B_H(t)]$ is statistically indistinguishable from $r^{-H}[B_H(t + rT) - B_H(t)]$ for any T and any $r > 0$. The variance of FBM obeys the power law

$$\mathrm{Var}[B_H(t + T) - B_H(t)] = V_H T^{2H} \tag{80}$$

where V_H is a constant depending on H. The fractal dimension of $B_H(t)$ is $D = 2 - H$. Its power spectrum[7] is

$$S_H(\omega) \propto \frac{1}{|\omega|^{2H+1}} \tag{81}$$

Hence, an efficient algorithm (Voss, 1988) to synthesize an FBM is to create a random sampled spectrum whose average magnitude is $1/|\omega|^{H+0.5}$ and its random phase is uniformly distributed over $[0, 2\pi]$. In our experiments we synthesized and then transformed this spectrum via an inverse FFT to obtain an FBM sequence from which we retained the first $N + 1$ samples. Figure 1*c* shows synthesized FBM sequences of varying D. The larger D (the smaller H), the more fragmented these fractal signals look.

In addition to the FFT method, there are several other methods to synthesize FBM signals (Mandelbrot and Wallis, 1969; Voss, 1988). One rigorous approach discussed by Lundahl *et al.* (1986) involves Cholesky decomposition of the correlation matrix of discrete fractional Gaussian noise (i.e., sequence of increments of FBM) and synthesizing the FBM as a running average of the fractional noise. This approach, however, is computationally more complex than the FFT approach.

Some special methods to measure D for FBM signals include:

1. Fitting a straight line to the data $(\log S_H(\omega), \log|\omega|)$ and measuring the slope yields D. This is perhaps the most popular method because of the simplicity of computing spectra using FFT. The power spectrum estimation part of this approach has been improved in various ways which include using Gabor filters (for 2D FBM) by Super and Bovik (1991) and wavelet decomposition of $1/|\omega|^{\beta}$ processes in noise (Wornell and Oppenheim, 1990).
2. The statistical self-affinity of FBM yields a power scaling law for many of its moments; linear regression on these data can measure D (Pentland, 1984).
3. Maximum likelihood methods for estimating the H of discrete fractional Gaussian noise have been developed by Lundahl *et al.* (1986) and by Tewfik and Deriche (1991).

[6] In Barnsley (1988) and in Mazel and Hayes (1991) more general FIFs are also discussed using hidden variables.

[7] Strictly speaking, the power spectrum of the nonstationary FBM is not well-defined. However, for $\omega \neq 0$, we can approximately interpret $S_H(\omega)$ as proportional to the average power of $B_H(t)$ within a narrow frequency band around ω (Mandelbrot, 1982).

4. Mallat (1989) showed that the ratio of the energies of the detail signals at any two consecutive scales in a dyadic wavelet decomposition of an FBM signal is equal to 2^{2^H}; this can be used to estimate H.

V. Measuring the Fractal Dimension of 1D Signals

A. 2D Covers via 2D Set Operations

In this section we focus on a generalized version of the Minkowski cover method. Specifically, given a nonempty compact set $B \subseteq \mathbf{R}^2$, consider the positive homothetics $\varepsilon B = \{\varepsilon b : b \in B\}$ at all scales $\varepsilon \geq 0$, and define the generalized cover $C_B(\varepsilon)$ of a planar set $F \subseteq \mathbf{R}^2$ as its morphological dilation by the structuring element εB:

$$C_B(\varepsilon) = F \oplus \varepsilon B. \tag{82}$$

Henceforth we call C_B a *morphological cover*. The Minkowski cover corresponds to using a disk for B.

Bouligand's work implies that the Minkowski–Bouligand dimension of a compact planar set F can also be obtained by replacing the disks in the Minkowski cover with arbitrarily shaped planar compact sets B that have a nonzero area, contain the origin, and possess a nonzero minimum (δ_B) and maximum (Δ_B) distance from the origin to their boundary. Specifically,

$$\left(\frac{\delta_B}{\Delta_B}\right)^2 < \frac{\text{area}[C_B(\varepsilon)]}{\text{area}(F_\varepsilon)} < \left(\frac{\Delta_B}{\delta_B}\right)^2 \tag{83}$$

Hence

$$\lambda[\text{area}(C_B(\varepsilon))] = \lambda[\text{area}(F_\varepsilon)] \tag{84}$$

Thus if we replace the Minkowski cover area in (45) with the area of the generalized cover C_B, the fractal dimension will remain the same.

B. 2D Covers via 1D Function Operations

In this section we deal only with continuous-time finite-length signals $f(t)$, $0 \leq t \leq T$, in which case the curve F of the discussion in Section III becomes the graph

$$\text{Gr}(f) = \{(t, f(t)) : 0 \leq t \leq T\} \tag{85}$$

of f. If (x, y) are the Cartesian coordinates of the plane $\mathbf{R}^2$, the time t-axis will henceforth coincide with the x-axis, whereas the signal amplitude $f(t)$ assumes values on the y-axis.

The discussion in Section V.A implies that the fractal dimension of $\text{Gr}(f)$ can be found by using general morphological covers

$$\begin{aligned} C_B(\varepsilon) &\triangleq \text{Gr}(f) \oplus \varepsilon B \\ &= \{(t + x, f(t) + y) : (t, f(t)) \in \text{Gr}(f),\ (x, y) \in \varepsilon B\} \end{aligned} \tag{86}$$

of the signal's graph with compact planar sets $B \subseteq \mathbf{R}^2$: The digital implementations of such morphological coverings by disk-like or other (e.g., horizontal line segment) structuring elements were done in Tricot *et al.* (1988) and in Dubuc *et al.* (1989) by viewing $\text{Gr}(f)$ as a binary image signal and dilating this binary image. However, this 2D processing of a 1D signal, on the one hand is unnecessary and on the other hand increases the requirements in storage space and the time complexity for implementing the covering method. Thus, for purposes of computational efficiency, it is desirable to obtain the area of C_B by using 1D operations on f, i.e., dilations and erosions of f by a function g with a compact support G. Specifically, for a properly chosen g, we could obtain the cover area by integrating the difference signal $f \oplus g - f \ominus g$. However, since f is defined only[8] over $[0, T]$ and the morphological cover C_B involves points t from outside this interval, we modify the cover and the signal operations $f \oplus g$, $f \ominus g$ to handle the boundaries of f properly. Thus, we replace the covers $C_B(\varepsilon)$ with their restriction on the vertical strip $[0, T] \times (-\infty, \infty)$, i.e., with the truncated morphological cover

$$C_B^*(\varepsilon) \triangleq [\text{Gr}(f) \oplus \varepsilon B] \cap ([0, T] \times (-\infty, \infty)) \tag{87}$$

We also modify the definitions of 1D dilations and erosions, so that they do not require any values of f outside $[0, T]$. Thus, we define the support-limited dilation and erosion of f by g with respect to a support set $S \subseteq \mathbf{R}$:

$$(f \oplus_S g)(t) \triangleq \sup_{x \in (\check{G}+t) \cap S} \{f(x) + g(t - x)\}, \qquad t \in S \tag{88}$$

$$(f \ominus_S g)(t) \triangleq \inf_{x \in (G+t) \cap S} \{f(x) - g(x - t)\}, \qquad t \in S \tag{89}$$

In what follows we shall find a proper g such that the integral of the difference signal between the support-limited dilation and the erosion of f by g is equal to the area of the set cover $C_B^*(\varepsilon)$ at all scales ε, if B satisfies certain constraints. The main theoretical result requires a series of individual steps explained next.

[8] Assuming that $f(t)$ is defined over all $t \in \mathbf{R}$ by setting $f(t) = -\infty$ for $t \notin [0, T]$, the erosion $f \ominus g$ computed as in (8) gives a signal that is not the (desirable) lower envelope of the morphological cover $\text{Gr}(f) \oplus B$.

First, for each scale $\varepsilon \geq 0$, the upper and lower envelope of the morphological set cover are defined respectively as the signals

$$U_\varepsilon(x) \triangleq \sup\{y: (x, y) \in C_B(\varepsilon)\} \tag{90}$$

$$L_\varepsilon(x) \triangleq \inf\{y: (x, y) \in C_B(\varepsilon)\} \tag{91}$$

Further, let us define a function

$$g(x) \triangleq \sup\{y: (x, y) \in B\} \tag{92}$$

and its ε-scaled version by

$$g_\varepsilon(x) \triangleq \sup\{y: (x, y) \in \varepsilon B\}, \qquad \varepsilon \geq 0 \tag{93}$$

Then we have the following result.

Lemma 9. (Maragos and Sun, 1991). *Let $f: S \to \mathbf{R}$ be a continuous function, where $S = [0, T]$. Let $B \subseteq \mathbf{R}^2$ be a compact set that is symmetric with respect to both the x- and the y-axis of the plane. Then*

$$\begin{aligned} U_\varepsilon(x) &= f \oplus_S g_\varepsilon(x) \\ L_\varepsilon(x) &= f \ominus_S g_\varepsilon(x) \end{aligned} \qquad 0 \leq x \leq T \tag{94}$$

Further, if we define the function-cover area

$$A_g(\varepsilon) \triangleq \int_0^T [(f \oplus_S g_\varepsilon) - (f \ominus_S g_\varepsilon)](x)\, dx \tag{95}$$

we have the following.

Theorem 10. (Maragos and Sun, 1991). *Let $f: S \to \mathbf{R}$ be a continuous function, where $S = [0, T]$. Let $B \subseteq \mathbf{R}^2$ be a compact set that is also single-connected (i.e., connected with no holes) and symmetric with respect to both the x- and the y-axis of the plane. Then*

$$area[C_B^*(\varepsilon)] = \int_0^T [U_\varepsilon(x) - L_\varepsilon(x)]\, dx \tag{96}$$

and thus the set-cover and function-cover areas are identical:

$$\text{area}[C_B^*(\varepsilon)] = A_g(\varepsilon) \tag{97}$$

Thus, instead of creating the cover of a 1D signal by dilating its graph in the plane by a 2D set B (which means 2D processing), the original signal can be filtered with an erosion and a dilation by a 1D function g. For example, if B is a unit-radius disk or rhombus, then

$$B = \{(x, y): x^2 + y^2 \leq 1\} \Rightarrow g(x) = \sqrt{1 - x^2}, \qquad |x| \leq 1 \tag{98}$$

$$B = \{(x, y): |x| + |y| \leq 1\} \Rightarrow g(x) = 1 - |x|, \qquad |x| \leq 1 \tag{99}$$

In a related work, Tricot *et al.* (1988) and Dubuc *et al.* (1989) showed that we can find D_M by using set covers C_B where B is the unit horizontal segment $[-1, 1] \times \{0\}$ and that

$$v(\varepsilon) = \int_0^T \left[\sup_{|y| \leq \varepsilon} \{f(x + y)\} - \inf_{|y| \leq \varepsilon} \{f(x + y)\} \right] dx, \tag{100}$$

which is called the *variation* of f, is equal to area$[C_B^*(\varepsilon)]$ if $B = [-1, 1] \times \{0\}$. Their result becomes a special case of Theorem 10. Specifically the assumptions of Theorem 10 allow for B to be equal to horizontal segments $[-w, w] \times \{0\}$, in which case $g(t) = 0$ for $t \in [-w, w]$ and $g(t) = -\infty$ for $|t| > w$. Thus the horizontal structuring element case corresponds to selecting a flat function g equal to zero on its support.

The following theorem shows that we can find the fractal dimension D_M of the signal's graph by using covers with functions g.

Theorem 11. *Let the function f and set B satisfy all the assumptions of Theorem 10, and also assume that $B \neq \{(0, 0)\}$. Then the Minkowski-Bouligand dimension of the graph of f is equal to*

$$D_M[\text{Gr}(f)] = 2 - \lambda(A_g) = \lim_{\varepsilon \to 0} \frac{\log[A_g(\varepsilon)/\varepsilon^2]}{\log(1/\varepsilon)} \tag{101}$$

Proof. Both in the case where B has nonzero area and possesses a nonzero minimum distance from the origin to its boundary (Bouligand, 1928), and in the case where B is the horizontal segment $[-1, 1] \times \{0\}$ (Dubuc *et al.*, 1989), D_M remains unchanged if we replace the area of the Minkowski cover by disks in (45) with the area of covers C_B by the above generalized compact sets B. Then the area of $C_B(\varepsilon)$ is equal to the sum of area$[C_B^*(\varepsilon)]$ plus some residual term that is due to dilations of the graph's boundary points. The infinitesimal order of this residual term is 2, because it scales proportionally to ε^2. Hence, since $\lambda[\text{area}(C_B)] = 2 - D_M \leq 1$, we can ignore the above residual term and use as cover area in (45) the area of the truncated cover. Then, Theorem 10 completes the proof, since it allows to replace the area of covers by sets with the area of covers by functions. (*Q.E.D.*)

In practice, assuming that $A_g(\varepsilon) \approx (\text{constant}) \cdot \varepsilon^\lambda$ for ε very close to 0 yields that

$$\log \frac{A_g(\varepsilon)}{\varepsilon^2} \approx D_M \cdot \log\left(\frac{1}{\varepsilon}\right) + \text{constant}, \qquad \text{as } \varepsilon \to 0 \tag{102}$$

This leads to the following practical algorithm to compute D_M in the discrete case.

C. Algorithm for Discrete-Time Signals

To estimate the fractal dimension of a discrete-time finite-length signal $f[n]$, $n = 0, 1, \ldots, N$, we must adapt our discussion in Section V.B. First, covers at discrete scales $\varepsilon = 1, 2, 3, \ldots, \varepsilon_{max}$ are used. The set $B_c \subseteq \mathbf{R}^2$ used for covers is also restricted to be convex, because then $\varepsilon B_c = B_c^{\oplus\varepsilon}$ for $\varepsilon = 0, 1, 2, \ldots$ where $B^{\oplus\varepsilon} \triangleq B \oplus B \ldots \oplus B$ (ε times). Hence, for B_c convex and integer ε, g_ε is equal to the ε-fold dilation of g with itself, denoted as

$$g^{\oplus\varepsilon} \triangleq g \oplus g \ldots \oplus g \qquad (\varepsilon \text{ times}) \tag{103}$$

Then it can be shown that

$$f \oplus_S g^{\oplus\varepsilon} = ((f \oplus_S g) \oplus_S g \ldots) \oplus_S g \tag{104}$$

$$f \ominus_S g^{\oplus\varepsilon} = (\underbrace{(f \ominus_S g) \ominus_S g \ldots) \ominus_S g}_{\varepsilon \text{ times}} \tag{105}$$

All the above ideas lead to the following algorithm for digitally implementing the morphological covering method using function covers (Maragos and Sun, 1991).

Step 1. Select a unit-radius discrete set $B \subseteq \mathbf{Z}^2$ that is a convex symmetric subset of the 3×3 square set of pixels with integer coordinates (n, m), which correspond to points (n, mv) in $\mathbf{R}^2$ where $v > 0$ is the vertical grid spacing. There are only three choices for such a B, and the corresponding $g[n]$ is a three-sample function:

1. If **B** is the 3×3-pixel square, the corresponding g is shaped like a rectangle:
$$g_r[-1] = g_r[0] = g_r[1] = h > 0 \tag{106}$$
2. If **B** is the five-pixel rhombus, then g is shaped like a triangle:
$$g_t[-1] = g_t[1] = 0, \qquad g_t[0] = h > 0 \tag{107}$$
3. If B is the three-pixel horizontal segment, then the corresponding g can be viewed as resulting either from g_t or from g_r by setting $h = 0$. In this case g is a flat function equal to zero on its support.

Step 2. Perform recursively the support-limited dilations and erosions of f by $g^{\oplus\varepsilon}$ at scales $\varepsilon = 1, 2, \ldots, \varepsilon_{max}$. That is, set $G = \{-1, 0, 1\}$, $S = \{0, 1, \ldots, N\}$, and use (88) and (104), which yield

$$\begin{aligned} f \oplus_S g[n] &= \max_{-1 \le i \le 1} \{f[n + i] + g[i]\}, \qquad \varepsilon = 1 \\ f \oplus_S g^{\oplus(\varepsilon+1)} &= (f \oplus_S g^{\oplus\varepsilon}) \oplus_S g, \qquad \varepsilon \ge 2. \end{aligned} \tag{108}$$

Likewise for the erosions $f \ominus_S g^{\oplus\varepsilon}$. The dashed lines in Fig. 2 show these multiscale erosions/dilations by the three different functions g.

Step 3. Compute the cover areas

$$A_g[\varepsilon] = \sum_{n=0}^{N} ((f \oplus_S g^{\oplus\varepsilon}) - (f \ominus_S g^{\oplus\varepsilon}))[n], \qquad \varepsilon = 1, \ldots, \varepsilon_{max} \le \frac{N}{2} \tag{109}$$

Step 4. Fit a straight line using least squares to the graph of $\log(A_g[\varepsilon]/(\varepsilon)^2)$ versus $\log(1/\varepsilon)$, for $\varepsilon = 1, 2, \ldots, \varepsilon_{max}$. The slope of this line gives us an approximate estimate of the fractal dimension of f, as implied by (102).

Although the shape of the structuring function g is not very crucial, its height h, however, plays an important role. Although h does not affect the morphological covering method in the continuous case, in the discrete case large h will sample the plot of (102) very coarsely and produce poor results. Thus small h are preferred for finer multiscale covering area distributions. However, the smaller h is, the more computations are needed to span a given signal's range. In addition, as noted by Mandelbrot (1985), the covering method with 2D discrete disks (as well as the box-counting dimension) greatly depends on the relationship between the grid spacing v and the dynamic range of f. Henceforth, we assume that v is approximately equal to the signal's dynamic range divided by the number of its samples. This is a good practical rule, because it attempts to consider the quantization grid in the domain and range of the function as square as possible. Further, whenever $h > 0$, we select $h = v$. Therefore, assuming that for an N-sample signal, its range has been divided into N amplitude levels, the above algorithm that uses function-cover areas A_g has a linear complexity $O(N\varepsilon_{max})$ with respect to the signal's length, whereas using set-cover areas with 2D sets yields quadratic complexity $O(N^2\varepsilon_{max})$; further, both approaches give the same dimension, as Theorem 10 implies.

Among previous approaches, the 1D version of the work in Peleg *et al.* (1984), Stein (1987), and Peli *et al.* (1989) corresponds to the morphological covering method using g_t with $h = 1$. The "horizontal structuring element method" in Tricot *et al.* (1988) and in Dubuc *et al.* (1989) corresponds to using $h = 0$.

The fractal dimension of the graph of f resulting from the morphological covering method using function-covers (in both the continuous and discrete case) has the following attractive properties. (See Maragos and Sun, 1991, for proofs.) If f is shifted with respect to its argument and/or amplitude, then its fractal dimension remains unchanged; i.e.,

$$f'(x) = f(x - x_0) + b \Rightarrow D_M[\mathrm{Gr}(f)] = D_M[\mathrm{Gr}(f')] \tag{110}$$

for arbitrary b, x_0. Further, if $h = 0$, then the fractal dimension estimated via erosions/dilations by a flat g also remains invariant with respect to any

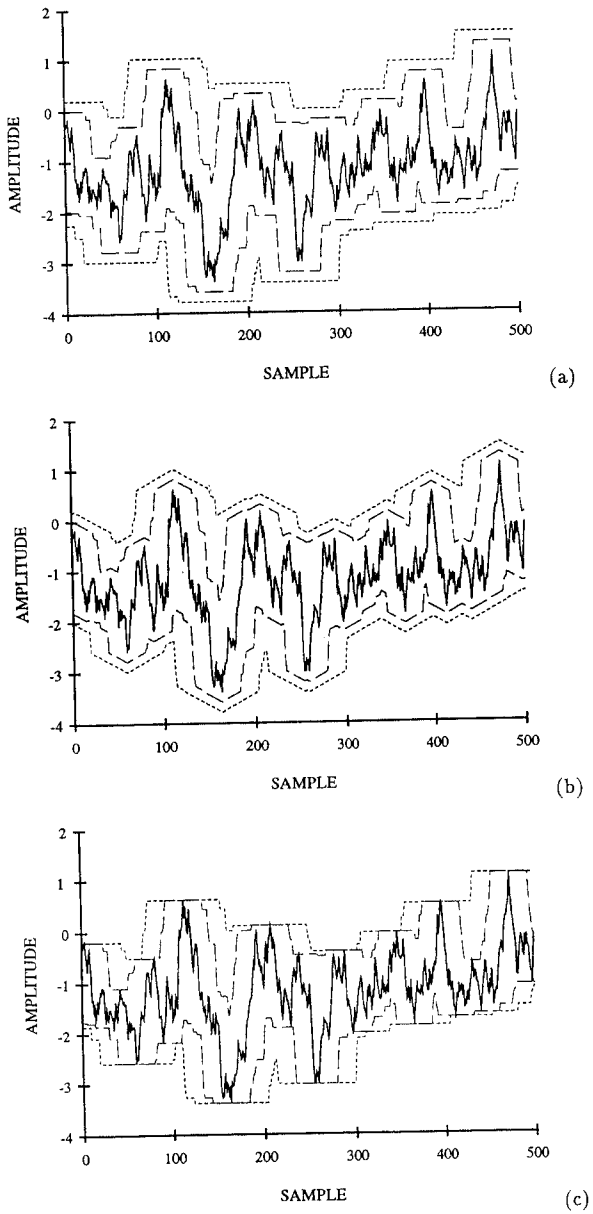

FIGURE 2. An FBM signal (solid line) with $D = 1.5$, $N = 500$, and its erosions/dilations (dashed lines) by $g^{\oplus\varepsilon}$ at scales $\varepsilon = 20, 40$. (a) Rectangular $g = g_r$ with $h = 0.01$. (b) Triangular $g = g_t$ with $h = 0.01$. (c) Rectangular g with $h = 0$. (From Maragos and Sun, 1991; ©1993 IEEE.)

affine scaling of the amplitude of f: i.e.,

$$f'(x) = af(x) + b \quad \text{and} \quad h = 0 \Rightarrow D_M[\mathrm{Gr}(f)] = D_M[\mathrm{Gr}(f')] \tag{111}$$

for arbitrary b and $a \neq 0$. The property (111) was also noted in Dubuc *et al.* (1989).

The morphological covering and the box counting method give identical fractal dimension for continuous-time signals f. However, in the discrete case they have different performances, and it is because of properties (110) and (111) that the morphological covering is more robust than the box counting method. The latter is affected by arbitrary shifts of the argument of f, by adding constant offsets to f, and (more seriously) by scaling its amplitude range, because all these affect the number of grid boxes intersected by the graph of f. However, the morphological covering method using covers with 1D functions g become completely independent from affine scalings of the signal's range if we choose $h = 0$. In addition, since for the case $h = 0$, the erosions/dilations by g can be performed faster, we henceforth set $h = 0$ in all our computer experiments with the morphological covering method.

Table 1 shows the estimated dimension D^* and the percent estimation error $100 \cdot |D - D^*|/D$ using a two-pass[9] morphological covering method on signals with $N + 1 = 501$ samples synthesized from sampling WCFs and FIFs of various D. The WCFs were defined for $t \in [0, 1]$ with $\gamma = 5$. The FIFs interpolated the six-point data sequence 0, 1, 4, 2, 5, 3 using positive scaling ratios $V = 5^{D-2}$. These experimental results and many others reported in Maragos and Sun (1991) indicate that, for these two classes of deterministic fractal signals, the morphological covering method performs very well for various combinations of dimensions $D \in [1.2, 1.8]$ and signal lengths $N \in [100, 2000]$ since the average percent error for estimating D was 2 to 3% for both WCFs and FIFs.

[9] The maximum scale ε_{max} and in general the scale interval $[1, \varepsilon_{max}]$ over which we attempt to fit a line to the log–log plot of (102) is an important parameter. The ε_{max} required for a good estimation of D may exhibit considerable variations and depends on the dimension D, on the signal's length N, and on the specific class of fractal signals. Maragos and Sun (1991) used the following heuristic rule for determining ε_{max}:

$$\varepsilon_{max} = MaxScale(D, N) = \min\left[\max\left(\frac{(D - 1.2)N}{1.5}, 10\right), \frac{N}{2}\right] \tag{112}$$

Thus, to apply the morphological covering method to a signal, a two-pass procedure consists of first applying the covering method with a small scale interval $\varepsilon_{max} = 10$, to obtain some estimate D_1 of the fractal dimension. Then the covering method is reapplied to the same signal by using $\varepsilon_{max} = MaxScale(D_1, N)$ to obtain a second estimate, which is considered as the final estimate D^* of D.

TABLE 1
MORPHOLOGICAL COVERING METHOD ON WCFS, FIFS, AND FBM

Signal	True D	Estimated	Error
WCF	1.4	1.424	1.71%
WCF	1.5	1.515	1.03%
WCF	1.6	1.606	0.39%
FIF	1.4	1.384	1.12%
FIF	1.5	1.478	1.45%
FIF	1.6	1.576	1.53%
FBM	1.4	1.393	0.5%
FBM	1.5	1.474	1.7%
FBM	1.6	1.553	2.9%

Table 1 also shows the results from applying the (two-pass) morphological covering method on FBM signals. For each true D, it reports the sample mean D^* of the estimates and the percent mean estimation error $100 \cdot |D - D^*|/D$ by averaging results over 100 random FBM realizations. All FBM signals had $N + 1 = 512$ samples and were synthesized using a 512-point FFT. Maragos and Sun (1991) compared the performance of the morphological covering method with that of the power spectrum method to estimate the fractal dimension of FBM signals in a noise-free case as well as in the presence of additive white Gaussian noise. Their experiments, over 7×5 combinations (D, N) of dimensions $D \in [1.2, 1.8]$ and signal lengths $N+1 \in \{2^7, 2^8, 2^9, 2^{10}, 2^{11}\}$ with 100 random FBM realizations each, indicate that in the absence of noise both methods yield a similar average error of about 3 to 4%, whereas in the presence of noise the morphological covering yields much smaller error than the power spectrum method.

Concluding, we emphasize that, since all three classes of fractal signals are sampled versions of nonbandlimited fractal functions, some degree of fragmentation is irreversibly lost during sampling. Hence, since the true D refers to the continuous-time signal, the discrete morphological covering algorithm (as well as any other discrete algorithm) can offer only an approximation of D. In addition, the specific approach used to synthesize the discrete fractal signals (e.g., the FFT for FBM) affects the relationship between the degree of their fragmentation and the true D, and hence it may also affect the performance of the D estimation algorithms.

D. *Application to Speech Signals*

The nonlinear dynamics of air flow during speech production may often result in some small or large degree of turbulence. In this section we quantify the geometry of speech turbulence, as reflected in the fragmentation of time signal, by using the short-time fractal dimension of speech signals. Some possible applications are also outlined for speech segmentation and sound classification.

During speech production a *vortex* is a flow region of similar (or constant) vorticity vector. Vortices in the speech air flow have been experimentally found above the glottis by Thomas (1986) and theoretically predicted in Teager and Teager (1989) and McGowan (1989) using simple geometries. There are several mechanisms for the creation of vortices: (1) velocity gradients in boundary layers; (2) separation of flow, which can easily happen at cavity inlets due to adverse pressure gradients; (3) curved geometry of tract boundaries, where due to the dominant inertia forces the flow follows the curvature and develops rotational components. After a vortex has been created, it can propagate downstream (Tritton, 1988) through vortex twisting and stretching as well as through diffusion of vorticity. The Reynolds number $\mathrm{Re} = \rho UL/\mu$ characterizes the type of flow, where U is a velocity scale; L is a typical length scale, e.g., the tract diameter; ρ is the air density; and μ is the air viscosity. As Re increases (e.g., in fricative sounds or during loud speech), all these phenomena may lead to instabilities and eventually result in *turbulent flow*, which is a "state of continuous instability" (Tritton, 1988) characterized by broad-spectrum rapidly varying (in space and time) velocity and vorticity. Modern theories that attempt to explain turbulence predict the existence of eddies (vortices with a characteristic size λ) at multiple scales. According to the energy cascade theory, energy produced by eddies with large size is transferred hierarchically to the small-size eddies that dissipate it due to viscosity. A related result is the famous Kolmogorov law,

$$E(k, r) \propto r^{2/3} k^{-5/3} \quad (k \text{ in a finite range}) \tag{113}$$

where $k = 2\pi/\lambda$ is the wavenumber, r is the energy dissipation rate, and $E(k, r)$ is the velocity wavenumber spectrum, i.e., Fourier transform of spatial correlations. In some cases this multiscale structure of turbulence can be quantified by fractals. Mandelbrot (1982) and others have conjectured that several geometrical aspects of turbulence (e.g., shapes of turbulent spots, boundaries of some vortex types found in turbulent flows, shape of particle paths) are fractal. In addition, processes similar to the ones that in high-Re speech flows cause vortices to twist, stretch, and fold (due to the bounded tract geometry) have also been found in low-order nonlinear dynamical systems to give rise to fractal attractors.

All the above theoretical considerations and experimental evidence motivated our use of fractals as a mathematical and computational vehicle to analyze and synthesize various degrees of turbulence in speech signals. The main quantitative idea that we focus on is the fractal dimension of

speech signals, because it can quantify their graph's fragmentation. Since the relationship between turbulence and its fractal geometry or the fractal dimension of the resulting signals is currently very little understood, herein we conceptually equate the amount of turbulence in a speech sound with its fractal dimension. Although this may be a somewhat simplistic analogy, we have found the short-time fractal dimension of speech to be a feature useful for speech sound classification and segmentation. To measure it, we use the morphological covering algorithm described in Section V.III with a flat function g, i.e., with height $h = 0$.

The speech signals used in our computer experiments were sampled at 30 kHz. Hence the smallest ($\varepsilon = 1$) time scale at which their fractal dimension D was computed was 1/15 msec. The dimension D was computed over moving speech segments of 30 msec ($N = 900$ samples) as a short-time feature. Figure 3 shows the waveform of a word and its short-time fractal dimension as function of time. While D behaves similarly with the average zero-crossings rate, it has several advantages: For example, it can distinguish between a vowel and a voiced fricative, whereas the zero-crossings can fail because the rapid fluctuations of the voiced fricative may not appear as zero-mean oscillations, which would increase the zero-crossing rate, but

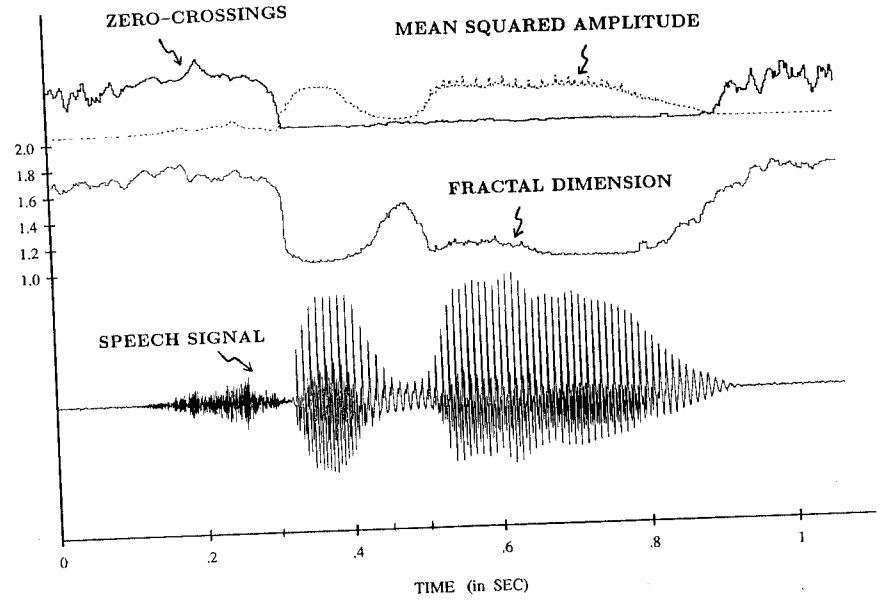

FIGURE 3. Speech waveform of the word /sieving/ sampled at 30 kHz and its short-time fractal dimension, average zero-crossings rate, and mean squared amplitude estimated over a moving 10 msec window, computed every 2 msec.

as a graph fragmentation that increases D. We have also observed cases where D could detect voiced stops but the zero-crossings could not. Thus, the short-time fractal dimension is a promising feature that can be used for segmentation of speech waveforms. However, as Fig. 3 shows, the silence portions of the signal (due to their noise-like geometrical structure) incur a high fractal dimension similar to that of the unvoiced fricatives. Therefore, for applying it to speech segmentation, the fractal dimension should be supplemented by some additional features that can distinguish between speech and silence.

Several experiments reported in Maragos (1991) lead to the following conclusions:

1. Unvoiced fricatives (*/F/*, */θ/*, */S/*), affricates, stops (during their turbulent phase), and some voiced fricatives like */Z/* have a high fractal dimension $\in [1.6, 1.9]$, consistent with the turbulence phenomena present during their production.
2. Vowels (at time scales < 0.1 msec) have a small fractal dimension $\in [1, 1.3]$. This is consistent with the absence or small degree of turbulence (e.g., for loud or breathy speech) during their production.
3. Some voiced fricatives like */V/* and */TH/*, if they don't contain a fully developed turbulence state, at scales < 0.1 msec have a medium fractal dimension $D \in [1.3, 1.6]$. Otherwise, their dimension is high (> 1.6), although often somewhat lower than that of their unvoiced counterparts.

Thus, for normal conversational speech, we have found that its short-time (e.g., over $\sim$ 10–30 msec frames) fractal dimension D (evaluated at a time scale < 0.1 msec) can roughly distinguish these three broad classes of speech sounds by quantifying the amount of their waveform's fragmentation. However, for loud speech (where the air velocity and Re increase, and hence the onset of turbulence is easier) or for breathy voice (especially for female speakers) the dimension of several speech sounds, e.g., vowels may significantly increase. In general, the D estimates may be affected by several factors including (a) the time scale, (b) the speaking state, and (c) the specific discrete algorithm for estimating D. Therefore, we often don't assign any particular importance to the absolute D estimates but only to their average ranges and relative differences.

Related to the Kolmogorov 5/3-law (113) is the fact that the variance of velocity differences between two points at distance ΔX varies $\propto (\Delta X)^{2/3}$. These distributions have identical form to the case of fractional Brownian motions whose variances scale with time differences ΔT as $(\Delta T)^{2H}$, $0 < H < 1$, the frequency spectra vary $\propto 1/|\omega|^{2H+1}$, and time signals are fractal with dimension $D = 2 - H$. Thus, putting $H = 1/3$ leads to $D = 5/3$

for speech turbulence. Of course, Kolmogorov's law refers to wavenumber (not frequency) spectra, and we dealt with pressure (not velocity) signals from the speech flow. Thus we should be cautious on how we interpret this result for speech. However, it is interesting to note that in our experiments with fricative sounds we often observed D (for time scales < 0.1 msec) in the range [1.65, 1.7]. Pickover and Khorasani (1986) reported a global dimension $D = 1.66$ for speech signals but no mention of the 5/3 law was made, their D estimation algorithm was different, and the time scales were much longer, i.e., 10 msec to 2 sec; thus in their work the time scales were above the phoneme level, whereas our work is clearly below the phoneme time scale.

VI. Measuring the Fractal Dimension of 2D Signals

A. 3D Covers via 3D Set Operations

Bouligand (1928) showed that the dimension D_M of compact sets $F \subseteq \mathbf{R}^3$ can also be obtained by replacing the spheres in the Minkowski cover with more generally shaped sets. Specifically, let B be a compact subset of $\mathbf{R}^3$ with Cartesian coordinates (x, y, z). Replacing the spheres of radius ε with the ε-scaled version of B, i.e., the positive homothetic $\varepsilon B = \{\varepsilon b : b \in B\}$ leads to the 3D morphological cover

$$C_B(\varepsilon) = F \oplus \varepsilon B \tag{114}$$

The Minkowski cover F_ε is a special case where B is a unit-radius sphere.

If B has a nonzero volume and its interior contains the origin, let us define the (nonzero) minimum and maximum distance from the origin to the boundary of B by δ_B and Δ_B, respectively. The Bouligand showed that

$$\left(\frac{\delta_B}{\Delta_B}\right)^3 < \frac{\text{vol}[C_B(\varepsilon)]}{\text{vol}(F_\varepsilon)} < \left(\frac{\Delta_B}{\delta_B}\right)^3 \tag{115}$$

Hence, the infinitesimal orders of $\text{vol}[C_B(\varepsilon)]$ and $\text{vol}(F_\varepsilon)$ are the same. Therefore, the fractal dimension of a set F can also be obtained from general morphological covers:

$$D_M(F) = 3 - \lambda[\text{vol}(C_B)] = \lim_{\varepsilon \to 0} \frac{\log(\text{vol}[C_B(\varepsilon)]/\varepsilon^3)}{\log(1/\varepsilon)} \tag{116}$$

For the case of a continuous nonconstant function $f(x, y)$ Dubuc *et al.* (1988) showed that B does not have to have nonzero volume, but it can also be a square parallel to the x, y plane; they called this special case the "horizontal structuring element method."

Bouligand's result (116) also applies to the special case where the set F becomes equal to the graph of some real function $f(x, y)$. In this case, however, the digital implementation would require covering the image surface by 3D sets, which can be done by viewing $\text{Gr}(f)$ as a set in the 3D discrete space and dilating this set of voxels. However, this 3D processing of a 2D signal on the one hand is unnecessary and on the other hand increases the requirements in storage space and the time complexity for implementing the covering method. Thus, for purposes of computational efficiency, it is desirable to obtain the volume of $C_B(\varepsilon)$ by using 2D operations on $f(x, y)$, i.e., dilations $\oplus$ and erosions $\ominus$ of f by a structuring function $g(x, y)$. This is explained in the next section.

B. 3D Covers via 2D Function Operations

Let $f(x, y)$ be a continuous real-valued function defined on the rectangular support

$$S = \{(x, y) \in \mathbf{R}^2 : 0 \le x \le X,\ 0 \le y \le Y\} \tag{117}$$

and assuming its values on the z-axis. Dilating its graph $\text{Gr}(f)$ by εB yields the cover

$$\begin{aligned} C_B(\varepsilon) &= \text{Gr}(f) \oplus \varepsilon B \\ &= \{(p + a, q + b, f(p, q) + c) : (p, q) \in S,\ (a, b, c) \in \varepsilon B\} \end{aligned} \tag{118}$$

The goal here is to obtain the volume of this cover not by performing the above set dilation, but by first computing the cover's upper and lower envelopes via morphologically dilating and eroding f by a function g related to B and then obtaining the original cover volume by integrating the difference signal between these envelopes over S. Of course, certain restrictions have to be set on B. Specifically, let the cover's upper and lower envelope be defined respectively as the 2D signals

$$U_\varepsilon(x, y) = \sup\{z : (x, y, z) \in C_B(\varepsilon)\} \tag{119}$$

$$L_\varepsilon(x, y) = \inf\{z : (x, y, z) \in C_B(\varepsilon)\} \tag{120}$$

Since $f(x, y)$ is defined only over S, and computing $\text{vol}[C_B(\varepsilon)]$ involves points from outside this interval, we modify the signal operations $f \oplus g$, $f \ominus g$ so that they do not require any values of f outside S. Thus, we define the support-limited dilation and erosion of f by g with respect to a support $S \subseteq \mathbf{R}^2$:

$$(f \oplus_S g)(x, y) = \sup_{(p,q) \in [\check{G} + (x,y)] \cap S} \{f(p, q) + g(x - p, y - q)\}, \quad (x, y) \in S \tag{121}$$

$$(f \ominus_S g)(x, y) = \inf_{(p,q) \in [G + (x,y)] \cap S} \{f(p, q) - g(p - x, q - y)\}, \quad (x, y) \in S \tag{122}$$

Further, if we define the function g by

$$g(x, y) = \sup\{z: (x, y, z) \in B\} \tag{123}$$

and its ε-scaled version by

$$g_\varepsilon(x, y) = \sup\{z: (x, y, z) \in \varepsilon B\} \tag{124}$$

then the following is true.

Lemma 12. *If $B \subseteq \mathbf{R}^3$ is compact and symmetric with respect to the x, y, z-axes, then for each $\varepsilon \geq 0$,*

$$\begin{aligned} U_\varepsilon(x, y) &= f \oplus_S g_\varepsilon(x, y) \\ L_\varepsilon(x, y) &= f \ominus_S g_\varepsilon(x, y) \end{aligned} \qquad (x, y) \in S \tag{125}$$

Proof. Let

$$G = \{(x, y): (x, y, z) \in B\} = \mathrm{Spt}(g) \tag{126}$$

Since B is symmetric with respect to the x, y-axes, $g_\varepsilon(x, y) = g_\varepsilon(-x, -y)$ and $G = \check{G}$. Since B is symmetric with respect to the z-axis, $g_\varepsilon(x, y) \geq 0$ for all (x, y) in its domain εG. If

$$I(a, b) = \{c: (a, b, c) \in \varepsilon B\}$$

for any $(a, b) \in \varepsilon G$, then note that

$$\begin{aligned} \sup\{c: c \in I(a, b)\} &= g_\varepsilon(a, b) \\ \inf\{c: c \in I(a, b)\} &= -g_\varepsilon(a, b) \end{aligned}$$

To prove (94) we have

$$\begin{aligned} U_\varepsilon(x, y) &= \sup\{z: x = p + a, y = q + b, z = f(p, q) + c, (p, q) \in S, \\ &\qquad (a, b, c) \in \varepsilon B\} \\ &= \sup\{f(x - a, y - b) + c: (a, b) \in \varepsilon G \cap [\check{S} + (x, y)], c \in I(a, b)\} \\ &= \sup\{f(p, q) + g_\varepsilon(x - p, y - q): (x, y) \in S \cap [\varepsilon G + (p, q)]\} \\ &= (f \oplus_S g_\varepsilon)(x, y) \end{aligned}$$

Likewise,

$$\begin{aligned} L_\varepsilon(x, y) &= \inf\{z: x = p + a, y = q + b, z = f(p, q) + c, (p, q) \in S, \\ &\qquad (a, b, c) \in \varepsilon B\} \\ &= \inf\{f(x - a, y - b) + c: (a, b) \in \varepsilon G \cap [\check{S} + (x, y)], c \in I(a, b)\} \\ &= \inf\{f(p, q) - g_\varepsilon(x - p, y - q): (x, y) \in S \cap [\varepsilon G + (p, q)]\} \\ &= (f \ominus_S g_\varepsilon)(x, y) \quad (Q.E.D.) \end{aligned}$$

By using the support-limited dilations and erosions we cannot account for the volume of the part of the original cover $C_B(\varepsilon)$ outside the support of f but only for the volume of the truncated morphological cover

$$C_B^*(\varepsilon) = [\mathrm{Gr}(f) \oplus \varepsilon B] \cap [S \times (-\infty, \infty)] \tag{127}$$

In what follows we shall show that the volume

$$V_g(\varepsilon) \triangleq \int_0^X \int_0^Y [f \oplus_S g_\varepsilon - f \ominus_S g_\varepsilon](x, y)\, dx\, dy \tag{128}$$

resulting from integrating the difference signal between the support-limited dilation and the erosion of f by g is equal to the volume of the truncated cover at all scales, if B satisfies certain constraints.

Lemma 13. *If $B \subseteq \mathbf{R}^3$ is compact, symmetric with respect to the x, y, z-axes, and single-connected, then for each $\varepsilon \geq 0$,*

$$\mathrm{vol}[C_B^*(\varepsilon)] = \int_0^X \int_0^Y [U_\varepsilon(x, y) - L_\varepsilon(x, y)]\, dx\, dy \tag{129}$$

$$= V_g(\varepsilon) \tag{130}$$

Proof. Since $g_\varepsilon(0, 0) \geq 0$, it can be easily shown that

$$U_\varepsilon(x, y) \geq f(x, y) \geq L_\varepsilon(x, y), \qquad (x, y) \in S$$

Define the set

$$Q(\varepsilon) = \{(x, y, z): (x, y) \in S, L_\varepsilon(x, y) \leq z \leq U_\varepsilon(x, y)\}$$

We shall prove that $Q(\varepsilon) = C_B^*(\varepsilon)$. First, let $(x, y, z) \in C_B^*(\varepsilon)$. Then, $(x, y) \in S$ and $(x, y, z) \in \mathrm{Gr}(f) \oplus \varepsilon B$. Hence, $x = p + a$, $y = q + b$, and $z = f(x, y) + c$ for some $(p, q) \in S$ and $(a, b, c) \in \varepsilon B$. But then, from the definition of U_ε, it follows that $z \leq U_\varepsilon(x, y)$; likewise, $z \geq L_\varepsilon(x, y)$. Therefore, $(x, y, z) \in Q(\varepsilon)$, and thus $C_B^*(\varepsilon) \subseteq Q(\varepsilon)$.

Now let $(x, y, z) \in Q(\varepsilon)$. Define the set

$$\begin{aligned} K &= \varepsilon B \cap [(\check{S} + (x, y)) \times (-\infty, +\infty)] \\ &= \{(a, b, c): (a, b) \in \varepsilon G \cap (\check{S} + (x, y)), c \in I(a, b)\} \end{aligned}$$

Then, K is a connected set. Define the function

$$\phi(a, b, c) = f(x - a, y - b) + c$$

on K. The function ϕ is continuous and has a connected domain K. The value z lies between the maximum $U_\varepsilon(x, y) = \sup\{\phi(a, b, c): (a, b, c) \in K\}$ and the minimum $L_\varepsilon(x, y) = \inf\{\phi(a, b, c): (a, b, c) \in K\}$ value of ϕ on K. Hence, from Bolzano's intermediate value theorem (Bartle, 1976, p. 153),

there is a point (a', b', c') in K at which ϕ takes the value z. By setting $p = x - a'$, $q = y - b'$, and $f(p, q) = z - c'$ we have $(p, q, f(p, q)) \in \mathrm{Gr}(f)$ and $(a', b', c') \in \varepsilon B$. Hence $(x, y, z) \in C_B^*(\varepsilon)$ and thus $Q(\varepsilon) \subseteq C_B^*(\varepsilon)$. Therefore, we proved that $Q(\varepsilon) = C_B^*(\varepsilon)$. This set equality proves (129). The result (130) follows from (129) and Lemma 12. Thus the proof is complete. (*Q.E.D.*)

Thus, instead of creating the cover of a 2D signal by dilating its graph by a 3D set B (which means 3D processing), the original signal can be filtered with an erosion and a dilation by a 2D function g. As an example, if $B = \{(x, y, z): x^2 + y^2 + z^2 \le 1\}$ is the unit-radius sphere, then

$$g(x, y) = \sqrt{1 - x^2 - y^2}, \qquad x^2 + y^2 \le 1.$$

Theorem 14. *Let $f: S \to \mathbf{R}$ be a continuous function, where*

$$S = [0, X] \times [0, Y] \subseteq \mathbf{R}^2.$$

Let $B \subseteq \mathbf{R}^3$ be a compact set that is also single-connected, symmetric with respect to the x, y, z-axes, and assume $B \neq \{(0, 0, 0)\}$. Then the Minkowski–Bouligand dimension of the graph of f is equal to

$$D_M[\mathrm{Gr}(f)] = 3 - \lambda(V_g) = \lim_{\varepsilon \to 0} \frac{\log[V_g(\varepsilon)/\varepsilon^3]}{\log(1/\varepsilon)} \tag{131}$$

Proof. Both in the case where (a) B has nonzero volume and possesses a nonzero minimum distance from the origin to its boundary (Bouligand, 1928), and in the case where (b) B is the horizontal unit square (Dubuc *et al.*, 1988), D_M remains unchanged if we replace the volume of the Minkowski cover by spheres in (39) with the volume of covers C_B by the above generalized compact sets B. Now, if $\partial\mathrm{Gr}(f)$ is the boundary of $\mathrm{Gr}(f)$, then the volume of $C_B(\varepsilon)$ is equal to

$$\mathrm{vol}[C_B(\varepsilon)] = \mathrm{vol}[C_B^*(\varepsilon)] + \mathrm{vol}[\partial\mathrm{Gr}(f) \oplus \varepsilon B]$$

The infinitesimal order of the volume of the dilated graph boundary is two, because it scales proportionally to ε^2. For example, in case (a) let δ_B and Δ_B be the minimum and maximum distance from the origin to the boundary of B. Then

$$\frac{\pi l(\delta_B \varepsilon)^2}{2} \le \mathrm{vol}[\partial\mathrm{Gr}(f) \oplus \varepsilon B] \le \frac{\pi l(\Delta_B \varepsilon)^2}{2}$$

where l is the (assumed finite) length of the boundary of $\mathrm{Gr}(f)$. Hence, since $\lambda[\mathrm{vol}(C_B)] = 3 - D_M \le 1$, we can ignore the term $\mathrm{vol}[\partial\mathrm{Gr}(f) \oplus \varepsilon B]$ and use as cover volume in (116) the volume of the truncated cover. Then, Lemma 13 completes the proof, since it allows to replace the volume of covers by sets with the volume of covers by functions. (*Q.E.D.*)

C. Discrete Algorithm

In practice we deal with 2D functions that are both quantized and spatially sampled, e.g., digital images. Thus, the theory in section VI.B must be adapted as follows. Assume that we have a 2D discrete-space finite-support signal $f[n, m]$, $n = 0, 1, \ldots, N$, $m = 0, 1, \ldots, M$. We shall use covers at discrete scales $\varepsilon = 1, 2, 3, \ldots, \varepsilon_{max}$. The 3D set $B_c \subseteq \mathbf{R}^3$ used for covers, in addition to the restrictions of Theorem 14, is also restricted to be convex so that its corresponding function g at integer scales ε is given by the ε-fold dilation $g^{\oplus\varepsilon} = g \oplus g \ldots \oplus g$. The 3D space is then assumed to be sampled by the cubic grid (n, m, k) of integer coordinates corresponding to the real coordinates (n, m, kv) where $v > 0$ is the grid spacing. We assume that v is approximately equal to the dynamic range of f divided by the average number of samples in one dimension. Finally, the discrete set $B \subseteq \mathbf{Z}^3$ corresponding to B_c is assumed to have a unit-radius, because larger radii would create coarser volume distributions. Hence, B must be a convex, symmetric subset of the $3 \times 3 \times 3$ set of voxels around the origin. This yields only six choices for B:

1. B is the 27-voxel cube with horizontal cross-section the 3×3-pixel square $G_s \subseteq \mathbf{Z}^2$, and the corresponding function g has square support and cubic shape:
$$g_{sc}[n, m] = \begin{cases} h > 0, & [n, m] \in G_s \\ -\infty, & [n, m] \notin G_s \end{cases} \tag{132}$$
2. B is the 11-voxel octahedron with horizontal cross-section the square G_s, and the corresponding function g has a square support and pyramid shape:
$$g_{sp}[n, m] = \begin{cases} 0, & [n, m] \in G_s \backslash \{(0, 0)\} \\ h > 0, & [n, m] = [0, 0] \\ -\infty, & [n, m] \notin G_s \end{cases} \tag{133}$$
3. B is the 15-voxel rhomboid with horizontal cross-section the five-pixel rhombus $G_r \subseteq \mathbf{Z}^2$, and the corresponding function g has a rhombus support and cubic shape:
$$g_{rc}[n, m] = \begin{cases} h > 0, & [n, m] \in G_r \\ -\infty, & [n, m] \notin G_r \end{cases} \tag{134}$$
4. B is the seven-pixel rhombo-octahedron with horizontal cross-section the rhombus G_r, and the corresponding function g has rhombus support and pyramid shape:
$$g_{rp}[n, m] = \begin{cases} 0, & [n, m] \in G_r \backslash \{(0, 0)\} \\ h > 0, & [n, m] = [0, 0] \\ -\infty, & [n, m] \notin G_r \end{cases} \tag{135}$$

5. B is the nine-voxel square $G_s \times \{0\}$. The corresponding function g is flat and can be obtained from the functions g_{sc} or g_{sp} by setting their heights $h = 0$.
6. B is the five-voxel rhombus $G_r \times \{0\}$. The corresponding function g is flat and can be obtained from the functions g_{rc} or g_{rp} by setting their heights $h = 0$.

The morphological covering algorithm for 2D signals consists of the following steps:

Step 1. Select a 3D set structuring element B from the above six choices, and let g be its corresponding function.

Step 2. Perform recursively the support-limited dilations and erosions of f by $g^{\oplus\varepsilon}$ at scales $\varepsilon = 1, 2, \ldots, \varepsilon_{max}$. That is, set G equal to G_s or G_r, $S = \{0, 1, \ldots, N\} \times \{0, 1, \ldots, M\}$, and use (121) and (104). If $G = G_s$, this yields for $\varepsilon = 1$

$$f \oplus_S g[n, m] = \max_{-1 \le i \le 1} \max_{-1 \le j \le 1} \{f[n + i, m + j] + g[i, j]\}$$

Then, for any G,

$$f \oplus_S g^{\oplus(\varepsilon+1)} = (f \oplus_S g^{\oplus\varepsilon}) \oplus_S g, \qquad \varepsilon \ge 2.$$

Likewise for the erosions $f \ominus_S g^{\oplus\varepsilon}$.

Step 3. Compute the volumes

$$V_g[\varepsilon] = \sum_{n=0}^{N} \sum_{m=0}^{M} ((f \oplus_S g^{\oplus\varepsilon}) - (f \oplus_S g^{\oplus\varepsilon}))[n, m]$$

Step 4. Fit a straight line using least-squares to the plot of

$$(\log V_g[\varepsilon]/\varepsilon^3, \log 1/\varepsilon).$$

The slope of this line gives an estimate of the fractal dimension of the graph of f.

Among previous approaches, the work in Peleg *et al.* (1984); Stein (1987); and Peli *et al.* (1989) corresponds to using g_{sp} or g_{rp} with $h = 1$. The variation method in Dubuc *et al.* (1988) corresponds to using a horizontal square B, i.e., a flat function g_{sp} with $h = 0$.

Assuming that $M = N$ and $v = (\max_{n,m}\{f[n, m]\} - \min_{n,m}\{f[n, m]\})/N$, the computational complexity of using covers with 3D sets is $O(N^3\varepsilon_{max})$, whereas using covers with 2D functions yields a complexity $O(N^2\varepsilon_{max})$. (In both cases, if $h > 0$, it is assumed that $h = v$.)

VII. Modeling Fractal Images Using Iterated Function Systems

There is a rich class of nonlinear dynamical systems that consists of combinations of contraction maps on the Euclidean space and converge to attractor sets that are fractals. These fractal attractors include many of the well-known mathematical fractal sets and can model well images of natural scenes. These systems are known as *iterated function systems* and their theory was developed mainly by Hutchinson (1981) and Barnsley (1988) and his coworkers.

Currently, there are many computer algorithms to generate fractals. Examples include the FFT-based synthesis of images modeled as 2D fractional Brownian motion (Voss, 1988) and the synthesis via iterated function systems (Barnsley and Demko, 1985; Diaconis and Shahshahani, 1986). However, the inverse problem, i.e., given a fractal image find a signal model and an algorithm to generate it, is much more important and very difficult. An approach that is promising for solving this inverse problem is modeling fractal images with collages; the basic theory is summarized in Section VII.A. Then an algorithm is described in Section VII.B to find the collage model parameters via morphological skeletonization.

A. Modeling Fractals with Collages

The key idea in the collage modeling (Barnsley *et al.*, 1986) of a fractal set F is that if we can closely cover it with a collage of m small patches that are reduced distorted copies of F, then we can approximately reconstruct F (within a controllable error) as the attractor of a set of m contraction maps (each map is responsible for one patch). To simplify the analysis let us assume that we deal with compact planar sets $F \subseteq \mathbf{R}^2$. Let $w_i: \mathbf{R}^2 \to \mathbf{R}^2$ be contraction maps; i.e.,

$$\|w_i(x) - w_i(y)\| \le s_i\|x - y\|, \qquad \forall\, x, y \in \mathbf{R}^2 \tag{136}$$

where $0 \le s_i < 1$ are constant contractivity factors. Let $\mathcal{K}$ be the collection of all nonempty compact subsets of $\mathbf{R}^2$ and define the collage map $W: \mathcal{K} \to \mathcal{K}$ by

$$W(X) \triangleq \bigcup_{i=1}^{m} w_i(X) = \bigcup_{i=1}^{m} \{w_i(x) : x \in X\}, \qquad X \in \mathcal{K} \tag{137}$$

Then Hutchinson (1981) showed that the map W is a contraction map on $\mathcal{K}$ with respect to the Hausdorff metric h, defined by

$$h(X, Y) \triangleq \inf\{r \ge 0 : X \subseteq Y \oplus rB, Y \subseteq X \oplus rB\}, \qquad X, Y \in \mathcal{K} \tag{138}$$

where B is the unit-radius disk. Namely

$$h(W(X), W(Y)) \le s \cdot h(X, Y) \tag{139}$$

where the contractivity factor s is equal to

$$s = \max_{1 \le i \le m} \{s_i\} \tag{140}$$

Thus, the contraction mapping theorem implies that, if we iterate the map W starting from any initial set $X \in \mathcal{K}$, a unique fixed point

$$\mathcal{A} = \lim_{n \to \infty} W^{on}(X) = W(\mathcal{A}) \tag{141}$$

will be reached. The limit set $\mathcal{A}$, called the *attractor*, is independent of the initial set X and is often a fractal set.

The following theorem goes one step further and states that if we can approximate well (with respect to the Hausdorff metric) an original set F with the collage $W(F)$ of an iterated function system $\{w_i : i = 1, \ldots, m\}$, then the attractor of this system will also approximate well the original set F.

Theorem 15. (Barnsley *et al.*, 1986). *Given a set $F \in \mathcal{K}$, if*

$$h(F, W(F)) < \varepsilon \tag{142}$$

then, for any $X \in \mathcal{K}$,

$$h\left(F, \lim_{n \to \infty} W^{on}(X)\right) < \frac{\varepsilon}{1 - s} \tag{143}$$

Thus, if we can find maps w_i that have small contractivities (i.e., $s \ll 1$) and make a good collage (i.e., with small distance ε), then by iterating on an arbitrary compact set X the collage map W we can synthesize in the limit an attractor set that approximates well the original set F.

In practical applications, analytically simple choices for the maps w_i are the affine maps

$$w_i\begin{pmatrix} x \\ y \end{pmatrix} = r_i \cdot \begin{bmatrix} \cos\theta_i & -\sin\theta_i \\ \sin\theta_i & \cos\theta_i \end{bmatrix} \begin{bmatrix} x \\ y \end{bmatrix} + \begin{bmatrix} t_{xi} \\ t_{yi} \end{bmatrix} \tag{144}$$

Each w_i, operating on all points (x, y) of F, gives a version of F that is rotated by an angle θ_i, shrunk by a scale factor r_i, and translated by the vector (t_{xi}, t_{yi}).

The collage theorem and a related synthesis algorithm have been very successful for fractal image modeling and coding (Barnsley, 1988). These ideas work very well for images that have considerable degree of self-similarity. The difficulty, however, lies in finding appropriate maps w_i, which (by variation of their scaling, rotation, and translation parameters) can collage F well. The majority of earlier solutions required either considerable human intervention or exhaustive searching of all parameters in a discretized space. An approximate solution to this problem has been provided for binary images by Libeskind-Hadas and Maragos (1987) who used the morphological skeleton transform to efficiently extract the parameters of these affine maps, as explained in the next section.

The collage models have also been extended to gray-level images by modeling image functions as measures and using the Hutchinson metric to quantify the goodness of the collage approximation (Barnsley, 1988). This measure-theoretic framework, however, is difficult to apply to images with discrete-domain. Recent improvements of the gray-level collage models for images with discrete-domain include the works of Jacquin (1992) and Lundheim (1992). Lundheim has also developed a least-squares approach to find optimal collage parameters, which is efficient and mathematically tractable.

B. Finding the Collage Parameters via Morphological Skeletons

First we summarize the morphological skeleton transform for binary images, and then we outline its usage for finding the collage parameters.

Since the *medial axis transform* (also known as symmetric axis or skeleton transform) was first introduced by Blum (1967), it has been studied extensively for shape representation and description, which are important issues in computer vision. Among the many approaches (Rosenfeld and Kak, 1982) to obtain the medial axis transform, it can also be obtained via erosions and openings (Mott-Smith, 1970; Lantuejoul, 1980; Serra, 1982; Maragos and Schafer, 1986). Let $F \subseteq \mathbf{Z}^2$ represent a finite discrete binary image, and let $B \subseteq \mathbf{Z}^2$ be a binary structuring element containing the origin. The nth skeleton component of F with respect to B is the set

$$S_n = (F \ominus nB) \setminus [(F \ominus nB) \bigcirc B], \qquad n = 0, 1, \ldots, N \tag{145}$$

where $N = \max\{n : F \ominus nB \neq \emptyset\}$ and $\setminus$ denotes set difference. The S_n are disjoint subsets of F, whose union is the morphological skeleton of F. (If B is a disk, then the morphological skeleton becomes identical with the medial axis.) We define the morphological skeleton transform of F to be the finite sequence $(S_0, S_1, \ldots, S_N)$. From this sequence we can reconstruct F exactly or partially; i.e.,

$$F \bigcirc kB = \bigcup_{k \le n \le N} S_n \oplus nB, \qquad 0 \le k \le N \tag{146}$$

Thus, if $k = 0$ (i.e., if we use all the skeleton subsets), $F \bigcirc kB = F$ and we have exact reconstruction. If $1 \le k \le N$, we obtain a partial reconstruction,

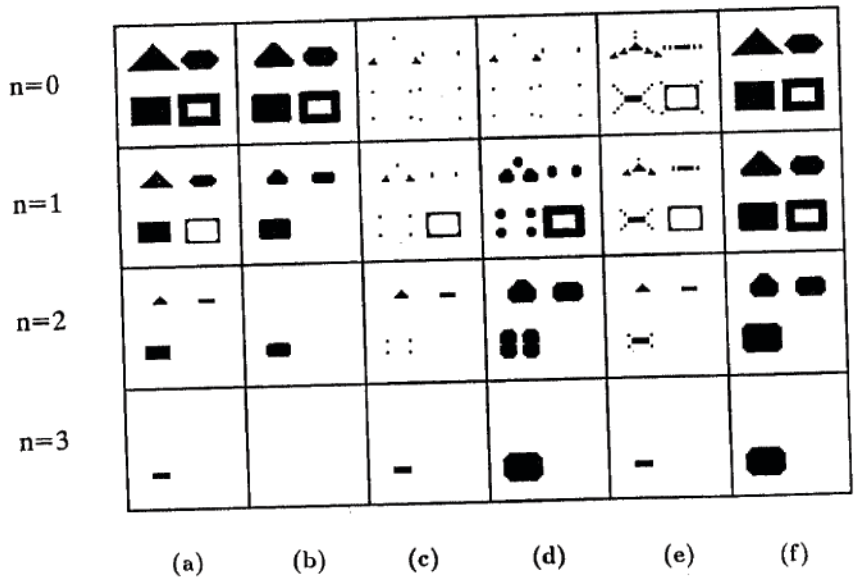

FIGURE 4. Morphological skeletonization of a binary image F (top left image) with respect to a 21-pixel octagon structuring element B. (a) Erosions $F \ominus nB$, $n = 0, 1, 2, 3$; (b) openings of erosions $(F \ominus nB) \bigcirc B$. (c) Skeleton subsets S_n. (d) Dilated skeleton subsets $S_n \oplus nB$. (e) Partial unions of skeleton subsets $\bigcup_{N \geq k \geq n} S_k$. (f) Partial unions of dilated skeleton subsets $\bigcup_{N \geq k \geq n} S_k \oplus kB$. (From Maragos and Schafer, 1986; © 1986 IEEE.)

i.e., the opening (smoothed version) of F by kB. The larger the size index k, the larger the degree of smoothing. Figure 4 shows a detailed description of the skeletal decomposition and reconstruction of an image. Thus, we can view the S_n as *shape components*. That is, skeleton components of small size indices n are associated with the lack of smoothness of the boundary of F, whereas skeleton components of large indices n are related to the bulky interior parts of F that are shaped similarly to nB.

Libeskind-Hadas and Maragos (1987) used the information in the morphological skeleton transform in the following way to obtain the collage model parameters. First note (referring to the notation of Section VII.A) that the collage theorem does not change if the collage map W is modified to contain a fixed condensation set C:

$$W(F) = C \bigcup_{i=1}^{m} w_i(F) \tag{147}$$

The set C is set equal to the dilation of the skeleton subset S_N corresponding to the largest scale index. This will model the bulky parts of the interior of an image F. (The origin of the plane is set equal to the mass centroid of S_N.) Then, every major skeleton branch is associated with a map w_i.

The translation vector (t_{xi}, t_{yi}) is taken as the vector of pixel coordinates of the skeleton branch point b. (The selection of the major skeleton branch points, which also determines the number of affine maps, is the only part of the algorithm done by visual inspection.) The rotation angle θ_i is found as the angle that the skeleton branch forms with the horizontal. (Estimates of the rotation angle can also be obtained from fitting a line via least-squares to several known points on the specific branch.) Finally, the scaling factor is set equal to $r = n/N$, where n is the index of the skeleton subset containing b. This algorithm can model images F that exhibit some degree of self-similarity; i.e., when local details of F closely resemble F as a whole.

Figure 5 shows an example of the application of morphological skeletonization to find the parameters of a collage model for the fractal

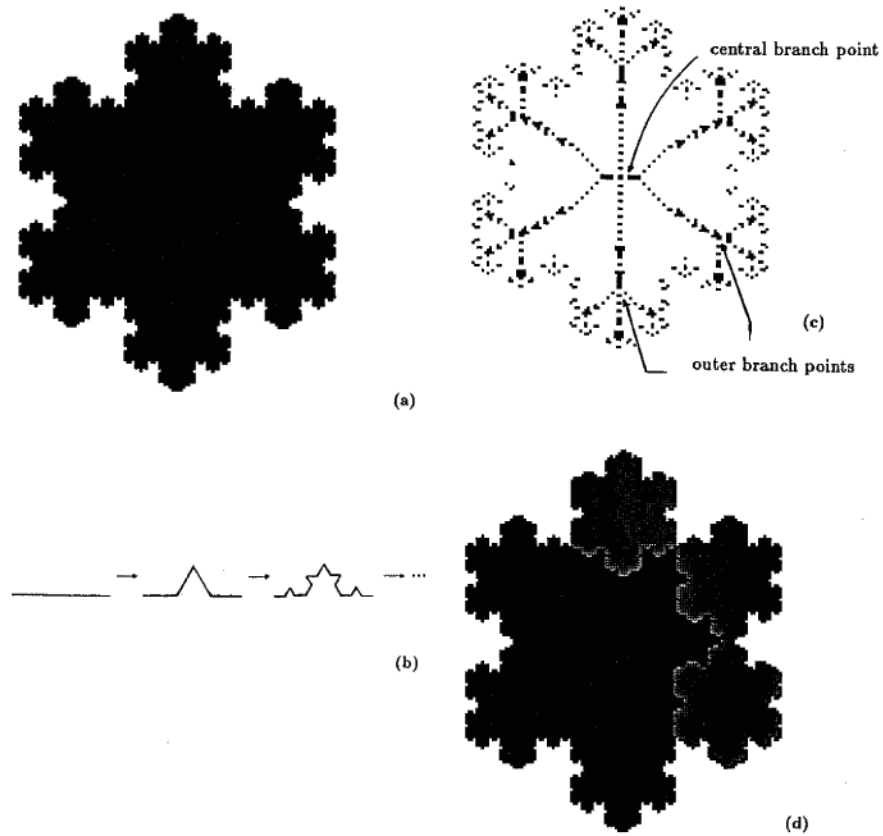

FIGURE 5. (a) Original binary image F (fractal Koch island). (b) Recursive process to construct the boundary of F. (c) Morphological skeleton of F (using a discrete disk for B). (d) Three of the six affine transformations of F. (From Libeskind-Hadas and Maragos, 1987; © 1987 SPIE.)

image of a Koch island. (The boundary of this 2D fractal set is generated through the recursive process of Fig. 5b and has similarity dimension log(4)/log(3).) Note that, due to the rotational symmetry of the Koch island with respect to its center, the rotation angles can also be set equal to zero in this example. Since the Koch island can be perfectly modeled as a collage of six affine maps (scaled by $r = 1/3$) and a large disk in the middle as condensation set, the attractor synthesized from the corresponding iterated function system is identical to the original image.

VIII. Conclusions

In this chapter two important aspects of fractal signals have been analyzed using concepts and operations from morphological signal processing: the measurement of the fractal dimension of 1D and 2D signals and the modeling of binary images as attractors of iterated systems of affine maps.

The major emphasis of the discussion was on the fractal dimension measurement. In this area a theoretical approach was presented for measuring the fractal dimension of arbitrary continuous-domain signals by using morphological erosion and dilation function operations to create covers around a signal's graph at multiple scales. A related algorithm was also described for discrete-domain signals. This morphological covering approach unifies and extends the theoretical aspects and digital implementations of several other covering methods. Many empirical experiments on synthetic fractal signals indicate that the performance of this method is good since it yields average estimation errors in the order of 0 to 4%. It also has a low computational complexity, which is linear with respect to both the signal's size of support and the maximum scale. It can be implemented very efficiently by using morphological filtering and can yield results that are invariant with respect to shifting the signal's domain and affine scaling of its dynamic range. The latter advantage makes the morphological covering method more robust than the box-counting method in the digital case. An interesting area of future research could be the investigation of the performance of this method in the presence of noise.

Modeling binary images with large degree of self-similarity as the attractors of iterated systems of affine maps is very promising for applications. However, efficient methods must be developed to find the parameters of these affine maps. A preliminary approach toward this goal was described based on the morphological skeleton transform. This approach is promising but it needs further work in automating the part for finding good branch points to place the collage patches; using connected skeletons may help finding such branch points. In addition, for the collage of an image F, improved rotation angles and scaling factors for each affine map w_i can be found by searching in a relatively small discretized space around the initial estimates found via morphological skeletonization and minimizing the area difference between F and $(F \bigcirc kB) \cup w_i(F)$, where k is a smoothing scale at which the fractal details do not exist. An extension of these idea to gray-level images using gray-level skeletonization could also be interesting.

Overall, the main characteristic of the morphological signal operators that enables them to be efficient in measuring the fractal dimension or finding the collage model parameters is their ability to extract information about the geometrical structure of signals at multiple scales.

Acknowledgments

This chapter was written while the author was a visting professor at the National Technical University of Athens, Greece. The research work reported herein was supported by the U.S. National Science Foundation's Presidential Young Investigator Award under the NSF Grant MIPS-86-58150 with matching funds from Xerox, and in part by the National Science Foundation Grant MIP-91-20624.

References

Barnsley, M. F. (1986). "Fractal Interpolation," *Constr. Approx.* **2**, 303–329.

Barnsley, M. F. (1988). *Fractals Everywhere*. Academic Press, Boston.

Barnsley, M. F., and Demko, S. (1985). "Iterated Function Systems and the Global Construction of Fractals," *Proc. Royal Soc. London* **A-399**, 243–275.

Barnsley, M. F., Ervin, V., Hardin, D., and Lancaster, J. (1986). "Solution of an Inverse Problem for Fractals and Other Sets," *Proc. National Acad. Sci.* **83**, 1975–1977.

Bartle, R. G. (1976). *The Elements of Real Analysis*. Wiley, New York.

Berry, M. V., and Lewis, Z. V. (1980). "On the Weierstrasse-Mandelbrot Fractal Function," *Proc. R. Soc. Lond. A* **370**, 459–484.

Besicovitch, A. S. (1934). "On the Sum of Digits of Real Numbers Represented in the Dyadic System. (On Sets of Fractional Dimension II)," *Math. Annalen* **110**, 321–329; "Sets of Fractional Dimension (IV): On Rational Approximation to Real Numbers," *J. London Math. Soc.* **9**, 126–131.

Besicovitch, A. S., and Ursell, H. D. (1937). "Sets of Fractional Dimension (V): On Dimensional Numbers of Some Continuous Curves," *J. London Math. Soc.* **12**, 18–25.

Blum, H. (1967). "A Transformation for Extracting New Descriptions of Shape." In *Models for the Perception of Speech and Visual Forms* (W. Wathen-Dunn, ed.), MIT Press, Cambridge, Massachusetts.

Bouligand, G. (1928). "Ensembles impropres et nombre dimensionnel," *Bull. Sci. Math.* **II-52**, 320–344, 361–376; *Bull. Sci. Math.* **II-53**, 185–192, 1929.

Diaconis, P. M., and Shahshahani, M. (1986). "Products of Random Matrices and Computer Image Generation," *Contemporary Mathematics* **50**, 173–182.

Dubuc, B., Zucker, S. W., Tricot, C., Quiniou, J. F., and Wehbi, D. (1988). "Evaluating the Fractal Dimension of Surfaces," Tech. Report TR-CIM-87-19, Computer Vision & Robotics Lab. McGill University, Montreal, Canada, July.

Dubuc, B., Quiniou, J. F., Roques-Carmes, C., Tricot, C., and Zucker, S. W. (1989). "Evaluating the Fractal Dimension of Profiles," *Phys. Rev. A* **39**, 1500–1512.

Falconer, K. (1990). *Fractal Geometry: Mathematical Foundations and Applications*. John Wiley & Sons, New York.

Farmer, J. D., Ott, E., and Yorke, J. A. (1983). "The Dimension of Chaotic Attractors," *Physica* **7D**, 153–180.

Hadwiger, H. (1957). *Vorlesungen über Inhalt, Oberfläche, und Isoperimetrie*. Springer Verlag, Berlin.

Haralick, R. M., Sternberg, S. R., and Zhuang, X. (1987). "Image Analysis Using Mathematical Morphology," *IEEE Trans. Pattern Anal. Mach. Intell.* **PAMI-9**, 523–550.

Hardin, D. P., and Massopust, P. R. (1986). "The Capacity for a Class of Fractals Functions," *Commun. Math. Phys.* **105**, 455–460.

Hardy, G. H. (1916). "Weierstrass's Non-Differentiable Function," *Trans. Amer. Math. Soc.* **17**, 322–323.

Hausdorff, F. (1918). "Dimension and Ausseres Mass," *Math. Annalen* **79**, 157–179.

Heijmans, H. J. A. M., and Ronse, C. (1990). "The Algebraic Basis of Mathematical Morphology. Part I: Dilations and Erosions," *Comput. Vision, Graphics, Image Process.* **50**, 245–295.

Hutchinson, J. (1981). "Fractals and Self-Similarity," *Indiana Univ. Math. J.* **30**, 713–747.

Jacquin, A. (1992). "Image Coding Based on a Fractal Theory of Iterated Contractive Image Transformations," *IEEE Trans. Image Processing* **1**, 18–30.

Kolmogorov, A. N., and Tihomirov, V. M. (1961). "Epsilon-Entropy and Epsilon-Capacity of Sets in Functional Spaces," *Uspekhi Matematicheskikh Nauk (N.S.)* **14**, 3–86, 1959. Translated in *Trans. Amer. Math. Soc.* (Series 2), **17**, 277–364.

Libeskind-Hadas, R., and Maragos, P. (1987). "Application of Iterated Function Systems and Skeletonization to Synthesis of Fractal Images." In *Visual Communications and Image Processing II* (T. R. Hsing, ed.), *Proc. SPIE* **845**, 276–284.

Lantuejoul, C. (1980). "Skeletonization in Quantitative Metallography." In *Issues of Digital Image Processing* (R. M. Haralick and J. C. Simon, eds.). Groningen, Sijthoff and Noordhoff, The Netherlands.

Lundahl, T., Ohley, W. J., Kay, S. M., and Siffert, R. (1986). "Fractional Brownian Motion: A Maximum Likelihood Estimator and Its Application to Image Texture," *IEEE Trans. Med. Imag.* **MI-5**, 152–160.

Lundheim, L. (1992). "Fractal Signal Modeling for Source Coding," Ph.D. Thesis, Norwegian Inst. Technology, Trondheim, Norway.

Mallat, S. G. (1989). "A Theory for Multiresolution Signal Decomposition: The Wavelet Representation," *IEEE Trans. Pattern Analysis Machine Intelligence* **PAMI-11**, 674–693.

Mandelbrot, B. B. (1982). *The Fractal Geometry of Nature*. W. H. Freeman, New York.

Mandelbrot, B. B. (1985). "Self-Affine Fractals and Fractal Dimension," *Phys. Scripta* **32**, 257–260.

Mandelbrot, B. B., and van Ness, J. (1968). "Fractional Brownian Motion, Fractional Noise and Applications," *SIAM Review* **10**(4), 422–437.

Mandelbrot, B. B., and Wallis, J. R. (1969). "Computer Experiments with Fractional Brownian Motion. Parts 1–3," *Water Resources Research* **5**, 228–267.

Maragos, P. (1991). "Fractal Aspects of Speech Signals: Dimension and Interpolation." In *Proc. IEEE Int'l Conf. Acoust., Speech, and Signal Processing*, Toronto, May.

Maragos, P., and Schafer, R. W. (1986). "Morphological Skeleton Representation and Coding of Binary Images," *IEEE Trans. Acoust., Speech, Signal Process* **ASSP-34**, 1228–1244.

Maragos, P., and Schafer, R. W. (1987). "Morphological Filters—Part I: Their Set-Theoretic Analysis and Relations to Linear Shift-Invariant Filters," *IEEE Trans. Acoust. Speech, Signal Processing* **ASSP-35**, 1153–1169.

Maragos, P., and Schafer, R. W. (1990). "Morphological Systems for Multidimensional Signal Processing," *Proc. IEEE* **78**, 690–710.

Maragos, P., and Sun, F.-K. (1991). "Measuring the Fractal Dimension of Signals: Morphological Covers and Iterative Optimization," Technical Report 91-14, Harvard Robotics Lab., Harvard University. Also in *IEEE Trans. Signal Processing*, Jan. 1993.

Mazel, D. S., and Hayes, M. H., III (1991). "Hidden-Variable Fractal Interpolation of Discrete Sequences." In *Proc. IEEE Int'l Conf. Acoust., Speech, and Signal Processing*, Toronto, May 1991.

McGowan, R. S. (1989). "An Aeroacoustics Approach to Phonation," *J. Acoust. Soc. Am.* **83**(2), 696–704.

McMullen, C. (1984). "The Hausdorff Dimension of General Sierpinski Carpets," *Nagoya Math. J.* **96**, 1–9.

Minkowski, H. (1901). "Uber die Begriffe Lange, Oberflache und Volumen," *Jahresber. Deutch. Mathematikerverein* **9**, 115–121.

Minkowski, H. (1903). "Volumen und Oberflache," *Math. Annalen* **57**, 447–495.

Mott-Smith, J. C. (1970). "Medical Axis Transformations." In *Picture Processing and Psychopictorics* (B. S. Lipkin and A. Rosenfeld, eds.),. Academic Press, New York.

Peleg, S., Naor, J., Hartley, R., and Avnir, D. (1984). "Multiple Resolution Texture Analysis and Classification," *IEEE Trans. Pattern. Anal. Mach. Intell.* **PAMI-6**, 518–523.

Peli, T., Tom, V., and Lee, B. (1989). "Multi-Scale Fractal and Correlation Signatures for Image Screening and Natural Clutter Suppression." In *Proc. SPIE, Vol. 1199: Visual Communications and Image Processing IV*, pp. 402–415.

Pentland, A. P. (1984). "Fractal-Based Description of Natural Scenes," *IEEE Trans. Pattern Anal. Mach. Intell.* **PAMI-6**, 661–674.

Pickover, C., and Khorasani, A. (1986). "Fractal Characterization of Speech Waveform Graphs," *Comp. & Graphics* **10**, 000–000.

Rosenfeld, A., and Kak, A. C. (1982). *Digital Picture Processing*, vols 1 and 2. Academic Press, New York.

Serra, J. (1982). *Image Analysis and Mathematical Morphology*. Academic Press, New York.

Serra, J., and Vincent, L. (1992). "An Overview of Morphological Filtering," *Circuits, Systems and Signal Processing* **11**(1), 47–108.

Stein, M. C. (1987). "Fractal Image Models and Object Detection." In *Visual Communications and Image Processing II* (T. R. Hsing, ed.), *Proc. SPIE*, Vol. 845.

Sternberg, S. R. (1986). "Grayscale Morphology," *Comput. Vision, Graph., Image Proc.* **35**, 333–355.

Super, B. J., and Bovik, A. C. (1991). "Localized Measurement of Image Fractal Dimension Using Gabor Filters," *J. Visual Commun. and Image Represent.* **2**, 114–128.

Teager, H. M., and Teager, S. M. (1989). "Evidence for Nonlinear Production Mechanisms in the Vocal Tract," *Proc. NATO ASI on Speech Production and Speech Modelling*, France.

Tewfik, A. H., and Deriche, M. (1991). "Maximum Likelihood Estimation of the Fractal Dimensions of Stochastic Fractals and Cramer-Rao Bounds." In *Proc. IEEE Int'l Conf. Acoust., Speech, and Signal Processing*, Toronto, May.

Thomas, T. J. (1986). "A Finite Element Model of Fluid Flow in the Vocal Tract," *Comput. Speech & Language* **1**, 131–151.

Tricot, C., Quiniou, J. F., Wehbi, D., Roques-Carmes, C., and Dubuc, B. (1988). "Evaluation de la dimension fractale d'un graphe," *Revue Phys. Appl.* **23**, 111–124.

Tritton, D. J. (1988). *Physical Fluid Dynamics*, Oxford University Press, Oxford.

Voss, R. F. (1989). "Fractals in Nature: From Characterization to Simulation." In *The Science of Fractual Images* (H.-O. Peitgen and D. Saupe, eds.), Springer-Verlag.

Wornell, G. W., and Oppenheim, A. V. (1990). "Fractal Signal Modeling and Processing Using Wavelets." In *Proc. 1990 Digital Signal Processing Workshop*. Mohonk, New Paltz, New York.